

1 **A machine learning approach to quantify meteorological drivers of** 2 **~~recent~~ 2015-2019 ozone pollution in China**

3 Xiang Weng¹, Grant L. Forster^{1,2}, Peer Nowack^{1,3}

4
5 ¹ School of Environmental Sciences, University of East Anglia, Norwich, NR47TJ, UK

6 ² National Centre for Atmospheric Sciences, University of East Anglia, Norwich, NR47TJ, UK

7 ³ Grantham Institute – Climate Change and the Environment, Department of Physics, and the Data Science Institute, Imperial
8 College London, London SW7 2AZ, UK

9
10 *Correspondence to:* Xiang Weng (x.weng@uea.ac.uk)

11 **Abstract.** Surface ozone concentrations ~~have been~~ increasing in many regions of China from 2015 to 2019 ~~for the past few~~
12 ~~years, in contrast to policy driven declines in other key air pollutants such as particulate matter.~~ While the central role of
13 meteorology in modulating ozone pollution is widely acknowledged, its quantitative contribution remains highly uncertain.
14 Here, we use a data-driven machine learning approach to assess the impacts of meteorology on surface ozone variations in
15 China for ~~the years~~ 2015 to 2019, considering the months of highest ozone pollution from April to October. To quantify the
16 importance of various meteorological driver variables, we apply non-linear random forest regression (RFR) and linear ridge
17 regression (RR) to learn the relationships between meteorological variability and surface ozone in China, and contrast the
18 results to those obtained with the widely used multiple linear regression (MLR) and stepwise MLR. We show that RFR
19 outperforms the three linear methods when predicting ozone using ~~only~~ local meteorological predictor variables, as evident
20 from its higher coefficients of determination (R^2) with observations (0.5 to 0.6 across China) when compared to the linear
21 methods (typically $R^2=0.4-0.5$). This implies the importance of non-linear relationships between local meteorological factors
22 and ozone, which are not captured by linear regression algorithms. In addition, we find that including non-local meteorological
23 predictors can further improve the modelling skill of RR, particularly for southern China, where the averaged R^2 increases
24 from 0.47 to 0.6. Moreover, this improved RR shows a higher averaged meteorological contribution to the increase trend of
25 ozone pollution in that region, pointing towards an elevated ~~highlighting the~~ importance of large-scale meteorological
26 phenomena for ozone pollution in southern China ~~that region~~. Overall, RFR and RR are in close agreement concerning the
27 leading meteorological drivers behind regional ozone pollution. ~~For example, we find that temperature variations are the~~
28 ~~dominant meteorological driver for ozone pollution in Northern China (e.g., Beijing Tianjin Hebei region), whereas variations~~
29 ~~in relative humidity are the most important factor in Southern China (e.g., Pearl River Delta). Variability in surface solar~~
30 ~~radiation modulates photochemistry but was not considered as such in previous controlling factor analyses, and is found to be~~
31 ~~the most important predictor in the Yangtze River Delta and Sichuan Basin regions. In general, our~~ In line with expectations,
32 our analysis underlines that hot and dry weather conditions with high sunlight intensity are strongly related to high ozone
33 pollution across China, thus further validating our novel approach. In contrast to previous studies, we also highlight surface

34 ~~solar radiation as a key meteorological variable to be considered in future analyses. This further validates our novel approach~~
35 ~~to quantify the central role of meteorology. By contrasting-comparing our meteorology-based meteorological ozone~~ predictions
36 with ~~observed ozone values measurements~~ between 2015 and 2019, we estimate that almost half of the ~~2015-2019 observed~~
37 ozone trends across China might have been caused by meteorological variability ~~ies on average. We highlight that th~~ These
38 insights are of particular importance given possible increases in the frequency and intensity of weather extremes such as
39 heatwaves under climate change.

40 1 Introduction

41 ~~Surface ozone is an air pollutant that can induce severe harm to both human health and ecosystems (Lefohn et al., 2018;~~
42 ~~Lelieveld et al. 2015). In the troposphere, it is primarily produced through photochemically induced reaction chains involving~~
43 ~~volatile organic compounds (VOCs), nitrogen oxides (NO_x) and carbon monoxide (CO) (Monks et al., 2015; Jacob, 2000).~~
44 Over the last decade, Chinese policymakers have been successfully implementing air pollution control policies and strategies,
45 such as The Clean Air Action Plan in 2013 (Chinese State Council, 2013), to reduce harmful air pollutants. As a result, annual
46 mean concentrations of fine particulate matter (PM_{2.5}) have been reduced by 30% to 50% from 2013 to 2018 in China (Zhai et
47 al., 2019), alongside significant decreases in ~~anthropogenic emissions of ozone precursors air pollutants and ozone precursors~~
48 such as ~~nitrogen oxides (NO_x) and carbon monoxide (CO) with 21% and 23% reductions, respectively, from 2013 to 2017~~
49 (Zhai et al., 2019; Zheng et al., 2018). ~~However, -Despite decreasing trends in NO_x and CO-summertime surface ozone~~
50 concentrations have ~~still~~ been increasing from 2013 to 2019 at a rate of about 1.9 ppb yr⁻¹ on average across China, with a
51 faster rate of 3.3 ppb yr⁻¹ in the North China Plain (Li et al., 2020), ~~highlighting the urgent need for a better understanding of~~
52 ~~how ozone pollution could be addressed effectively.~~

53 ~~Surface ozone is an air pollutant that can induce severe harm to both human health and ecosystems (Lefohn et al., 2018;~~
54 ~~Lelieveld et al. 2015). In the troposphere, it is primarily produced through photochemically induced reaction chains involving~~
55 ~~volatile organic compounds (VOCs), NO_x and CO (Monks et al., 2015; Jacob, 2000). It is well-known that the effectiveness~~
56 of ozone production is strongly dependent on the atmospheric chemical regime (e.g., Squire et al., 2015, Archibald et al., 2020),
57 in which ozone production is mainly controlled by the abundance of NO_x or VOCs. Many urban and industrial regions in China
58 have been identified and categorized as being within the VOC-limited regime (Ou et al., 2016; Wang et al., 2017). Under these
59 circumstances, surface ozone reductions may require tighter controls on VOCs emissions together with continuous reductions
60 in NO_x, while significant reductions in NO_x emissions without simultaneous and adequate controls on VOCs could lead to
61 increased ozone pollution in the short term (Wang et al., 2019), ~~which could largely explain the recent increases in surface~~
62 ~~ozone across China. Notably, the total emissions of nonmethane volatile organic compounds (NMVOCs) have actually~~
63 ~~increased by 11% in 2017 compared to 2010 (Zheng et al., 2018).~~ Another factor ~~might be the role of the~~ large reductions in
64 PM_{2.5}, especially during the period of 2013 to 2017, because fewer particles could reduce the aerosol sink of ozone-producing
65 radicals such as hydroperoxyl (HO₂) (Li et al., 2019a). However, ~~the quantitative contribution to the increases of ozone from~~

66 [HO₂ uptake on aerosol remains uncertain \(e.g., Tan et al., 2020\)](#), and it is likely that this effect has become less important as
67 PM_{2.5} concentrations continue to decline (X. Chen et al., 2021; Li et al., 2019b).

68 In conjunction with the effects of changing ozone precursor emissions, the effect of meteorological conditions on ozone
69 concentrations should always be considered. ~~Previous work has identified~~ [It is well-known](#) that ozone variations are strongly
70 co-determined by meteorological factors such as incoming solar radiation, temperature, humidity, atmospheric stagnation, and
71 precipitation (e.g., Otero et al., 2018; Zhang et al., 2018; Lu et al., 2019a). For example, solar radiation is pivotal to the
72 photochemical production and destruction of ozone (Finlayson-Pitts and Pitts, 2000). Higher surface temperatures, and in
73 general tropospheric temperatures, change the chemical reaction rate of many ozone-relevant chemical reactions and will affect
74 biogenic emissions of VOCs such as isoprene and monoterpenes which are also important ozone precursors- (Lu et al., 2019a;
75 Doherty et al., 2013; Guenther et al., 1993; Xie et al., 2008; Archibald et al. 2020). Work by Lu et al. (2019b) further indicated
76 that hotter and drier weather conditions were the main drivers for background ozone increase in 2017 in major city clusters of
77 China. Similarly, Ma et al. (2019) suggested that high biogenic VOCs emissions and meteorological conditions indicative of
78 heatwaves such as high temperature, low wind speed, and no precipitation can elevate ozone pollution in the North China Plain
79 (NCP). Furthermore, studies by Wang et al. (2021) and Pu et al. (2017) also found enhanced ozone concentrations during
80 heatwaves in the Pearl River Delta (PRD) and Yangtze River Delta (YRD). Such links between meteorology and ozone
81 pollution provide clear evidence for the necessity to quantify the influence of meteorological factors or even climate change
82 on ozone pollution in China (e.g., Lu et al., 2019a; Meehl et al. 2018). Characterizing the major meteorological drivers behind
83 ozone variations in different regions of China will also be crucial for achieving effective mitigation of ozone pollution now
84 and under future changes in climate.

85 To quantify the importance [of](#) meteorological drivers, previous studies such as Li et al. (2019a) and Han et al. (2020)
86 adopted stepwise multiple linear regression (MLR) to derive linear relationships between meteorological factors and measured
87 surface ozone concentrations across China. Both of these studies demonstrated the significant skill of stepwise MLR in
88 modelling ozone and in quantifying the driver-response relationships. Nevertheless, a key limitation of stepwise MLR or
89 conventional MLR is that these methods are not able to accurately capture non-linearity, which is a severe constraint given
90 that non-linear relationships between meteorological factors and ozone, e.g., between temperature and ozone, are to be
91 expected (e.g., Pu et al., 2017; Gu et al., 2020; Archibald et al., 2020). In addition, MLR can suffer from [a](#) severe loss in
92 predictive skill and reliability in settings where a large number of (collinear) meteorological factors are considered as predictors
93 (cf., the curse of dimensionality in high-dimensional regression problems; Nowack et al., 2021; Bishop, 2006). Although the
94 stepwise MLR approach adopted by Li et al. (2019a) can overcome collinearity and overfitting to some extent ([i.e.](#), because
95 only a few predictors that are particularly strongly influencing ozone concentrations are kept), it is inevitable that many relevant
96 meteorological factors will be excluded from the final MLR predictions using ~~that~~ [such an](#) approach.

97 In order to capture [any](#) non-linear relationships between many meteorological factors and ozone and to overcome the
98 potential limitations of considering collinearity and high-dimensional settings in MLR, we will use a machine learning
99 approach as the next logical step to advance such controlling factor analyses of ozone pollution. Specifically, we will adopt

100 random forest regression (RFR) (e.g., Grange et al., 2018; Stirnberg et al., 2021) as a non-linear approach and contrast the
101 results to a linear statistical learning approach that is also robust in high-dimensional settings in the form of ridge regression
102 (RR) (e.g., Nowack et al., 2018). Both RFR and RR will also be compared with more conventional statistical methods such as
103 MLR and stepwise MLR.

104 Our paper is structured as follows. In Sect. 2, we describe the data used in this study and the modelling framework of the
105 two machine learning algorithms, namely, RFR and RR. In Sect. 3, the performances of RFR and RR will be discussed first
106 and then compared to those achieved with MLR and stepwise MLR. ~~Afterwards, we summarize~~ We then summarize the most
107 important meteorological drivers for surface ozone as identified by RFR and RR. Finally, we conduct a trend analysis of recent
108 surface ozone changes in China, and use our method to estimate the contribution of meteorological effects.

109 **2 Methods**

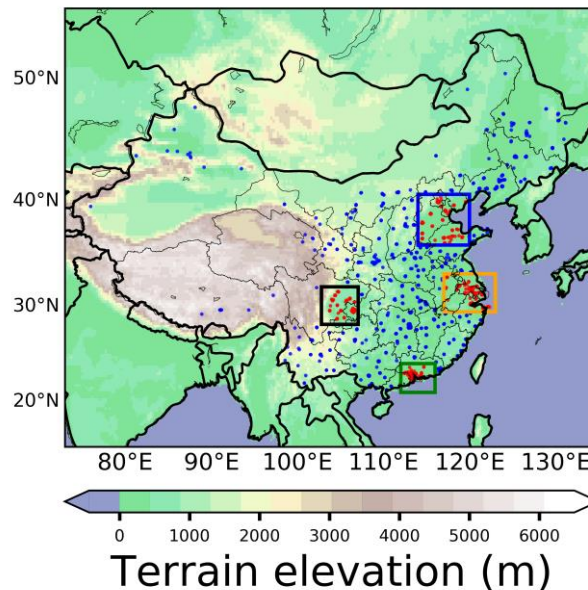
110 **2.1 Surface ozone and meteorological data**

111 The surface air quality measurement data used in this study were obtained from <https://quotsoft.net/air/> (Wang, X. L.,
112 2021; last accessed: 13 July 2021) which is a mirror of the data from the China Ministry of Ecology and Environment (MEE).
113 For the purposes of quantifying ozone pollution severity, we use the maximum daily 8-hour rolling mean (MDA8) ozone
114 calculated following the guidelines by the Ministry of Environmental Protection of [the](#) People’s Republic of China (MEP,
115 2012). The calculation selects the maximum value from [the](#) 8-hour rolling means of ozone for each station between 08:00 and
116 24:00 on each day. To be considered, each station must have a valid 14 hours data record of 8-hour rolling means [of](#) ozone
117 within 08:00 to 24:00 on ~~the a~~ the a respective day, otherwise, MDA8 ozone is not calculated for that day. Previous studies (e.g., Li
118 et al., 2020; Li et al., 2019a; Han et al., 2020) have focused on ozone pollution during the boreal summer months i.e., June,
119 July, and August (JJA) as the season with the most frequent occurrence of extreme ozone episodes in China. In this work, we
120 extend this analysis period to include the months from April to October to account for the fact that the seasonality of ozone
121 does not follow a uniform pattern across China. For example, peak ozone concentrations are often found during autumn ~~over~~
122 [in](#) the PRD region (Gao et al., 2020; see Fig. S1 in the Supplementary Material). In addition, we further constrain our analysis
123 to the period 2015 to 2019 to maintain greater consistency of the ozone data throughout our analysis period as the MEE
124 included far fewer measurement stations prior to 2015. In order to maintain consistency and reliability of all ozone data from
125 stations within the study period, only those stations with over 80% temporal coverage of MDA8 ozone data record in each
126 year are selected. For quality assurance of the data, we further examined each station’s MDA8 ozone variation individually
127 and noticed that measurements from some stations appeared to show a less reliable data record than others. This was for
128 example evident from extended periods of non-fluctuating ozone levels (see Fig. S2), or from sudden unusual MDA8 spikes,
129 usually followed by periods of suppressed ozone variability (see Fig. S3). According to our best judgement, such abrupt
130 changes or unrealistically low variability are unlikely to reflect actual ozone pollution profiles. Data from stations that showed

131 such unusual time evolutions were excluded from our analysis as to avoid the inclusion of unrealistic artefacts. The list of
132 stations that are not used in this study is summarized in Table S1.

133 To study regional meteorological drivers of ozone, we distinguish four regions of particularly high population density
134 known as Beijing-Tianjin-Hebei (BTH, ~~which is equivalent to north China plain~~), Yangtze River Delta (YRD), Pearl River
135 Delta (PRD) and Sichuan Basin (Sichuan), using definitions frequently used in previous studies (e.g., Li et al., 2019a; Han et
136 al., 2020). The boundaries of these four regions are adjusted to ensure that stations in each region have similar topography and
137 equivalent elevation. The four regions are also known as the target areas for air pollution reduction in Chinese government
138 plans (MEE; <http://www.mee.gov.cn/hjzl/dqhj/cskqzlkzyb/> last access: 1 December 2021; Li et al., 2019a). The locations of
139 stations within the four regions are indicated by red dots in Fig. 1.

140



141

142 **Figure 1. Elevation height (m) and locations of all ground-based stations and the four megacity cluster regions, BTH (blue box; 114°**
143 **E-120° E, 36° N-40.62° N), YRD (orange box; 117° E-123° E, 29.458° N-33.238° N), PRD (green box; 112° E-116° E, 21° N-24.111°**
144 **N), Sichuan Basin (black box; 102.8° E-107.061° E, 28.2° N-31.976° N). Red (blue) dots indicate [the](#) locations of stations within**
145 **(outside) the four regions.**

146 For the meteorological data, we use the gridded ERA5 reanalysis product (Hersbach et al., 2020) available at
147 <https://cds.climate.copernicus.eu/> (last accessed: 11 November 2021). Specifically, we use hourly data for a total of 11
148 meteorological variables at 0.25°×0.25° spatial resolution, namely, [the](#) temperature at 2 m (T2), boundary layer height (BLH),
149 mean sea level pressure (SLP), surface solar radiation downward (SSRD), relative humidity at 1000 hPa (RH), total
150 precipitation (TP), zonal wind at 10 m (U10), meridional wind at 10 m (V10), zonal wind at 850 hPa (U850hPa), meridional
151 wind at 850 hPa (V850hPa) and vertical velocity at 850 hPa (W850hPa) for the same time period as for the ozone station data.

152 Then the MDA8 ozone data are spatially averaged within the dimensions of each ERA5 grid cell to obtain the best possible
153 spatial match between the station-based ozone data and the large-scale meteorological factor data.

154 The variables of T2, BLH, SLP, RH, TP, U10, V10 can also be found as predictors in the controlling factor analyses
155 multi-linear/multilinear regression (MLR) from the studies of Han et al. (2020) and Li et al. (2019a). Surface solar radiation
156 downward (SSRD) is included in this study instead of adding a cloud coverage term as done by Han et al. (2020) and Li et al.
157 (2019a). Essentially, we consider SSRD to more directly characterize the local photochemical environment for ozone
158 production and loss than cloud coverage. Zonal and meridional wind at 10 m may be important for the dispersion of ozone's
159 precursors on a local scale. Both zonal and meridional winds s at 850 hPa are adopted in this study in order to encompass the
160 effect of transport of more polluted or cleaner air from remote regions. Wind at 850 hPa is less likely to be affected by
161 orography than wind at 10 m altitude, and it is thus better suited for considering the effect of larger-scale/larger-scale transport
162 and dispersion. Additionally, we represent the role of vertical transport of air masses by including vertical velocity at 850 hPa
163 as another factor.

164 2.2 Data pre-processing

165 Prior to modelling ozone, we pre-processed the meteorological data by averaging the raw hourly data over different
166 periods each day and this process is summarised in Table 1. The averaging periods were not the same for all meteorological
167 variables. For example, T2, SSRD, SLP, RH, and W850hPa are averaged between local time (UTC+8:00) 06:00 to 18:00 ~~on~~
168 each day. The average of these hours is sufficient to cover all daytime hours when ozone is photochemically produced from
169 April to October. ~~Total precipitation is calculated as the sum of accumulated precipitation for all hours from 06:00 to 18:00~~
170 Total precipitation is calculated by summing up all hourly accumulated precipitation (m) from 06:00 to 18:00. For zonal
171 and meridional wind at 10 m and 850 hPa, data are averaged over 06:00 to 12:00, which covers the main hours that may have
172 potential fresh emission of precursors and transport or dispersion of precursors or ozone. Boundary layer height (BLH) is
173 averaged over 00:00 to 12:00 for the consideration of both potential night-time emission of industrial activities when the
174 boundary layer is still low and transportation emission during morning rush hours. Through this process, raw hourly
175 meteorological data can be converted to a daily format, temporally matching with MDA8 ozone data. Finally, both ozone data
176 and meteorological data are deseasonalized. Specifically, for MDA8 ozone and the converted daily meteorological variables,
177 we first calculate 15-day moving window averages centered on the particular calendar date from 2015 to 2019. We then take
178 the difference between each day's MDA8 ozone or daily meteorological variables and these 15-day averages to obtain daily
179 anomalies, creating smooth time series of deseasonalized MDA8 ozone and deseasonalized meteorological variables.

180

181 **Table 1. Summary of the meteorological controlling factor variables and the respective times of day considered in their averages.**
182 **The motivation behind each selected time period is provided in the main text. Note: a positive zonal wind means westerly; positive**
183 **meridional wind means southerly; positive vertical velocity means downward motion.**

Acronyms	Names and units of variables	Average period
T2	temperature at 2 m (K)	06:00 to 18:00
SSRD	surface solar radiation downward (J m^{-2})	06:00 to 18:00
SLP	mean sea level pressure (Pa)	06:00 to 18:00
RH	relative humidity (%)	06:00 to 18:00
BLH	boundary layer height (m)	00:00 to 12:00
U10	zonal wind at 10m (m s^{-1})	06:00 to 12:00
V10	meridional wind at 10m (m s^{-1})	06:00 to 12:00
TP	total precipitation (m)	06:00 to 18:00 (sum)
U850hPa	zonal wind at 850_hPa (m s^{-1})	06:00 to 12:00
V850hPa	meridional wind at 850_hPa (m s^{-1})	06:00 to 12:00
W850hPa	vertical velocity at 850_hPa (Pa s^{-1})	06:00 to 18:00

184 ~~Finally, both ozone data and meteorological data are deseasonalized. Specifically, for MDA8 ozone and the converted~~
185 ~~daily meteorological variables, we first calculate 15-day moving window averages centered on the particular calendar date~~
186 ~~from 2015 to 2019. We then take the difference between each day's MDA8 ozone or daily meteorological variables and these~~
187 ~~15-day averages to obtain daily anomalies, creating smooth time series of deseasonalized MDA8 ozone and deseasonalized~~
188 ~~meteorological variables.~~

189 2.3 Machine learning methods for modelling MDA8 ozone

190 To model the relationships between meteorological variables and MDA8 ozone concentrations in China, we use two
191 regression algorithms, a non-linear approach known as random forest regression (RFR) and a linear approach called ridge
192 regression (RR). Within our framework, the predictors are the deseasonalized meteorological variables from ERA5 and the
193 dependent variable is the deseasonalized ground-based MDA8 ozone. For RR, both the deseasonalized meteorological
194 variables and the deseasonalized ozone time series are standard-scaled (normalized to zero mean and unit standard deviation)
195 as to avoid an imbalance of factors in the regularization part of the RR cost function (Nowack et al., 2018).

196 Both RFR and RR have been extensively described elsewhere (e.g., Nowack et al., 2018; Grange et al., 2018; Mansfield
197 et al., 2020; Nowack et al., 2021) and it is beyond the scope of this study to provide an in-depth description. Briefly, RFR is
198 based on learning an ensemble of decision trees, where each individual tree splits data into groups until reaching certain pre-
199 set definitions for data 'purity' (Breiman, 2001; Grange et al., 2018). RR is a least-squares linear regression method augmented
200 by L2-regularization with the goal to avoid overfitting in high-dimensional regression settings, especially in regression
201 problems with strong collinearity (McDonald, 2009). Both RFR and RR are known to handle collinearity comparatively well
202 (e.g., Dormann et al. 2013), which is key given that many of meteorological variables such as temperature and solar radiation
203 are correlated with each other. To assess whether these two machine learning algorithms can improve the accuracy of ozone

204 modelling compared to conventional statistical methods, we will contrast our results to multiple linear regression (MLR)– ~~that~~
205 ~~which~~ may not be highly capable of handling collinearity and overfitting and stepwise MLR. For MLR, we simply adopt the
206 same modelling framework of RFR and RR; all 11 meteorological variables are ingested into MLR as predictors. For stepwise
207 MLR, we adopted a similar approach as Li et al. (2019a): we start with 11 deseasonalized meteorological variables as predictors
208 in MLR and remove one predictor at a time based on the smallest significance of the regression coefficient in each new subset
209 of predictors; until there are only 3 meteorological predictors left. These 3 predictors are considered to be important predictors
210 and are used in the final model of stepwise MLR for modelling deseasonalized MDA8 ozone.

211 2.4 Training, testing and cross-validation in machine learning

212 Supervised machine learning approaches such as the two algorithms we use here ~~require involve~~ distinct training,
213 validation and testing phases to tune the relevant hyperparameters (explained in detail below) and to validate the skill of the
214 resulting predictive functions on new, unseen data not used in the training and tuning process (e.g., Bishop, 2006). During the
215 training phase, both predictors (i.e., deseasonalized meteorological variables) and dependent ~~variable–variables~~ (i.e.,
216 deseasonalized MDA8 ozone) are available and each machine learning regression algorithm is fit to this dataset, assuming
217 different combinations of values for the ~~hyperparamters~~ ~~hyperparameters~~ of each algorithm. The best objective ~~estimate for~~
218 ~~the~~ combination of hyperparameters is then found in the validation step by predicting ozone values for a validation dataset not
219 used at the training stage (e.g., for a different year in the data record). During the testing phase, the trained and validated
220 algorithm is used operationally to make new predictions for ozone values given a new dataset for the meteorological variables
221 as input to the machine learning function. These test set predictions can then be used to measure the “out-of-sample” skill of
222 the algorithm in predicting ozone pollution given certain meteorological conditions. In this study, we split the 5-years of data
223 (2015 to 2019) systematically into training/validation and testing datasets one at a time and in a rotating fashion. Specifically,
224 4 of these 5 years are classified as training/validation data, leaving 1 year for testing. To ensure that we are measuring the true
225 predictive performance and relationships, our predictive results and model evaluations are only conducted for the test data,
226 which has not been used at the training and validation stages. This process rotates until ozone data for each year have been
227 assigned once as test data so that all 5 years of data can be predicted by RFR and RR.

228 Machine learning regressions such as RFR and RR optimize their predictive performance by tuning certain sets of
229 hyperparameters. To determine the most suitable set of hyperparameters, we use a statistical cross-validation method. ~~Initially,~~
230 ~~we split the 5 years of data into 1 test year and 4 training/validation years. Specifically, For cross-validation,~~ the 4-year
231 training/validation set is further split into four folds (one year per fold). We then run a grid search over pre-defined
232 combinations of hyperparameters by training on three folds and predicting on the fourth fold in a classic 4-fold cross-validation
233 procedure. We finally select the ~~best-estimated~~ ~~best-estimated~~ set of hyperparameters on the basis of the average validation
234 data prediction performance as measured by the coefficient of determination (i.e., the R^2 ~~regression~~–score ~~function which is~~
235 ~~one of the metrics used in sklearn; see https://scikit-learn.org/stable/modules/generated/sklearn.metrics.r2_score.html, last~~
236 ~~access: 13 April 2022~~), and refit model coefficients using this set of hyperparameters for the entire 4 years of training/validation

237 data. We note that we avoid a ‘leave-one-out’ ~~cross-validation~~cross-validation method (in which only one daily sample is the
238 test dataset at a time) as we expect autocorrelation in our data—(i.e., MDA8 ozone may share similarity in adjacent dates),
239 which, intuitively, could lead to an overestimate of our predictive skill if testing data immediately follows training data points.

240 The ranges of hyperparameters we search over for both RFR and RR are set as follows. For RFR, the maximum depth for
241 trees growing is iterated in a step of 1 from 8 to 15. ~~Maximum-~~The maximum percentage of features and maximum samples
242 (with the bootstrap method) ~~are-is~~ set from 20% to 90% and 30% to 80% with 10% incremental steps, respectively. ~~Total-~~The
243 total tree number for the forest is set at 200 as a compromise between model complexity and runtime. Optimizations further
244 showed that the minimum samples per leaf is best set to 3 in our RFRs so that we finally kept this value constant in our grid
245 searches. In terms of RR, the regularization strength is iterated over a range of 1 to 199 with an incremental step of 2, which
246 appeared to encapsulate the best solution in each case. A detailed explanation of these hyperparameters for RFR and RR is for
247 example provided in Nowack et al. (2021).

248 **2.5 Identifying and quantifying importance of meteorological drivers**

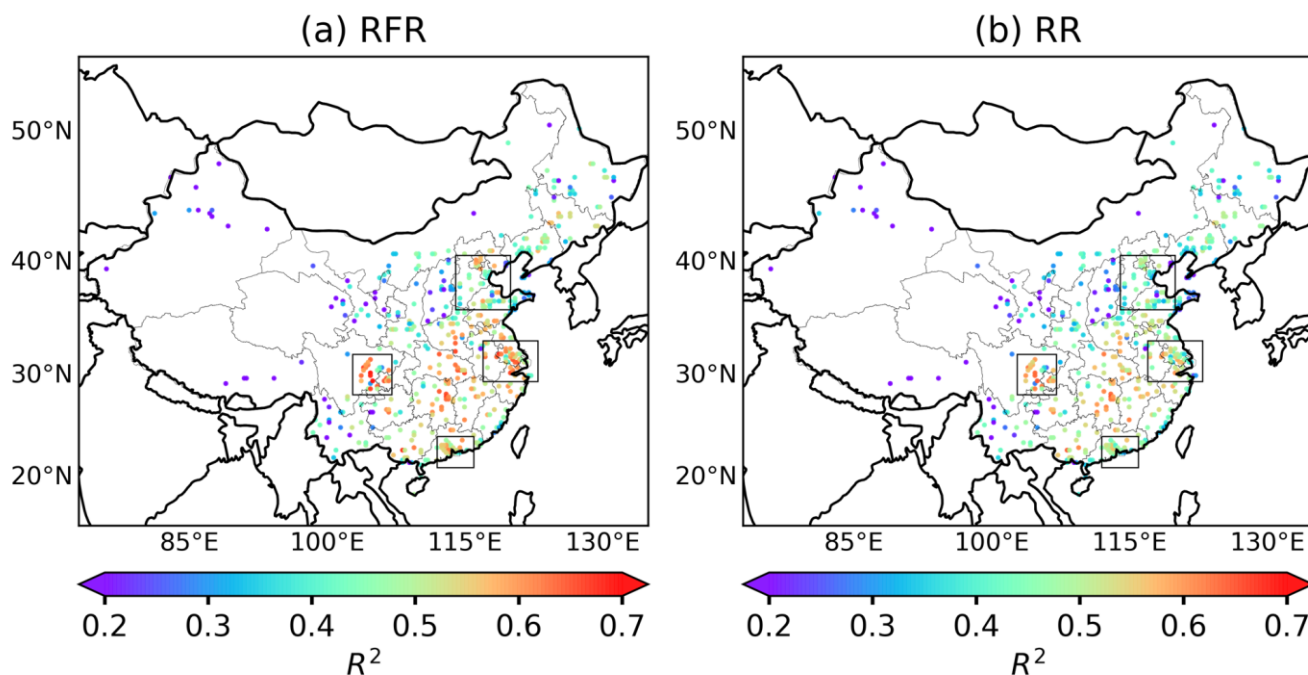
249 Both RFR and RR can enable the identification of the most important meteorological drivers for MDA8 ozone and can
250 help to quantitatively evaluate their relative importance. For RFR, we here measure the importance of each meteorological
251 predictor through a metric called Gini importance. A greater Gini importance implies a greater influence of a particular
252 predictor (i.e., the deseasonalized meteorological variable) on the dependent variable (i.e., deseasonalized MDA8 ozone) (e.g.,
253 Menze et al., 2009; Zhao et al., 2019, Kuhn-Régnier et al., 2021). Since we train the RFR five times ~~for-given~~ each possible
254 set of 4-year training/validation data, we average the Gini importance scores for each meteorological predictor across all five
255 runs for our final discussion below. For RR, similar to MLR, the importance of each predictor is evaluated by the magnitude
256 of each predictor’s averaged slope (linear regression coefficient) across all 4-year training/validation datasets, which represents
257 the linear effect of each predictor ~~onto-on~~ ozone, given that all predictors are standard-scaled (see Sect. 2.3).

258 **3 Results and discussion**

259 **3.1 Machine learning performances for modelling ozone using local meteorological predictors**

260 It is important to first assess how well ~~the selected of these~~ machine learning algorithms can model ozone by using only
261 meteorological variables as predictors. Therefore, we adopt the coefficient of determination (R^2) as a standard metric for the
262 evaluation of prediction performance, which assesses the goodness-of-fit for the linear regression between the deseasonalized
263 MDA8 ozone data and the predicted values (~~i.e., the square of Pearson correlation coefficient, R~~) ~~as a standard metric for~~
264 ~~prediction performance~~(~~e.g., Han et al., 2020~~)~~-on the deseasonalized MDA8 ozone data~~. As mentioned above, to measure the
265 true predictive skill of the machine learning functions, we only compare our predictions for out-of-sample test data that are
266 not used during training/validation stages against the deseasonalized measured MDA8 ozone data.

267 To begin with, the predictors used by RFR and RR ~~here~~ are only the local meteorological variables, i.e., each ERA5
 268 grid point's meteorological variables are used as predictors to model the averaged deseasonalized MDA8 ozone for that
 269 particular grid location. The average prediction performance of RFR and RR by comparing predictions across all test years
 270 against the deseasonalized measured MDA8 ozone data across China is illustrated in Fig. 2.



271
 272 **Figure 2. Coefficient of determination (R^2) between deseasonalized observational MDA8 ozone and deseasonalized predicted values**
 273 **in random forest regression (a) and ridge regression (b). The skill is only measured for the respective test datasets. Each dot**
 274 **represents the center of the ERA5 grid location, within which station values for MDA8 ozone are averaged.**

275 Overall, the model performance of RFR generally surpasses the one of RR over most regions of China, with higher R^2
 276 values in grid locations within the Sichuan Basin, YRD, PRD and other regions of southeast China. R^2 ~~scores-values~~ for RFR
 277 generally range from 0.5 to 0.6 across China while RR reaches R^2 ~~scores-values~~ from 0.4 to 0.5. RFR and RR perform similarly
 278 over the central region of BTH, while in the northern region of BTH (e.g., Beijing), R^2 values are still found to be higher in
 279 RFR than RR. The averaged R^2 across all ERA5 grid locations within BTH, YRD, PRD, and Sichuan Basin is 0.46, 0.56, 0.53
 280 and 0.57 respectively for RFR, which are all higher than the equivalent R^2 for RR (BTH: 0.41, YRD: 0.48, PRD: 0.47, Sichuan
 281 Basin: 0.53).

282 In order to examine whether RR can improve the model performance by ~~addressing overfitting being less sensitive to~~
 283 ~~collinearity~~, we also applied MLR with all 11 meteorological predictors and the stepwise MLR approach with the 3 most
 284 important meteorological factors in the final MLR for comparison ~~(see Sect. 2.3)~~. ~~Overall, Although most R^2 values across~~
 285 ~~China for~~ ~~these three linear regressions (i.e., RR, MLR and stepwise MLR) are within the same range of 0.4 to 0.5,~~ stepwise
 286 MLR ~~shows the worst performance with~~ ~~consistently lower R^2 values across China, and more of these values fall R^2 scores in~~

287 ~~a lower range ranging of from~~ 0.3 to 0.4, ~~across China, with~~. Moreover, the averaged R^2 ~~scores values for stepwise MLR in~~
288 BTH, YRD, PRD and Sichuan Basin ~~are found to be lower~~ at 0.39, 0.45, 0.43 and 0.52, respectively (see Fig. S4b in
289 Supplement for ~~the~~ spatial distribution of R^2 ~~scores values~~). This suggests that the stepwise MLR approach may carry a risk of
290 not including all important meteorological predictors in the regression model. However, RR does not show noticeable
291 improvements over MLR, as evident from similar regionally averaged R^2 ~~scores values~~ (see [Table 2](#) and Fig. S4a), suggesting
292 that the problem of collinearity is still limited given the use of 11 meteorological predictors. The enhanced performance of
293 RFR compared to RR may therefore be attributed to ~~the ability of RFR being able~~ to model non-linear relationships between
294 local meteorological variables and ozone, indicating that a flexible machine learning approach, such as RFR that can capture
295 non-linearity, is more suitable to reflect relationships between local meteorological factors and ozone.

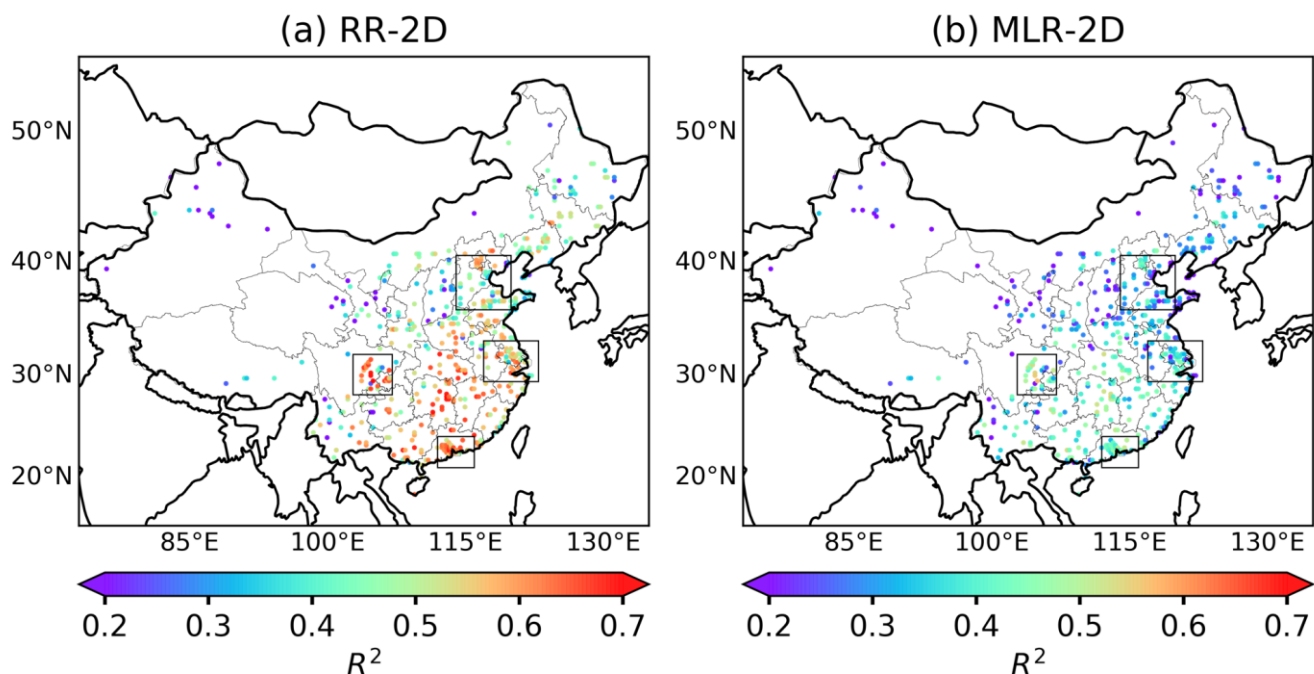
296 3.2 Predictive skill using additional non-local meteorological predictors

297 ~~Meteorological phenomena are usually belong related to the meteorology into a larger spatial context at a larger scale.~~
298 ~~Weather systems that affect ozone (e.g., For example, high-pressure systems) usually take in a larger spatial domains, driving~~
299 ~~regional temperature anomalies and suppressing or accelerating in air flow airflow~~ in certain directions. Consequently, it
300 seems intuitive that a meteorological controlling factor framework for ozone might benefit from including additional non-local
301 information in the regressions, i.e., if we were to consider surrounding meteorological context information that is not just
302 limited to the predicted ozone grid point in question (Ceppi and Nowack 2021).

303 We thus ran a second version ~~of our controlling factor analysis of our controlling factor analysis in which we did not just~~
304 ~~include local values of meteorological drivers, but additionally to investigate the~~ ~~consider a~~ spatially wider effect ~~of that~~
305 meteorology ~~may have~~ on a two-dimensional (2D) domain of meteorological variables. This is possible since both RR and
306 RFR ~~are less prone to better address~~ collinearity and overfitting in high-dimensional regression settings than simple non-
307 regularized MLR approaches ~~would be~~, meaning that the additional information included in the regressions might well
308 outweigh the cost of adding more predictors.

309 In detail, for each ozone target grid point, we include a meteorological context by adding each meteorological variable
310 within a $7.5^\circ \times 7.5^\circ$ rectangle domain around the center of this target grid point to the set of model predictors, i.e., all the
311 meteorological variables from the ERA5 $0.25^\circ \times 0.25^\circ$ grids within this $7.5^\circ \times 7.5^\circ$ rectangular domain are used as individual
312 predictors in the regression models. This adds potentially important information about the larger-scale meteorological situation
313 to our predictions, but also significantly increases the dimensionality (number of predictors) of our regression problem and
314 increases the number of collinear predictors. Indeed, we find that through the additional L2-regularization in RR with 2D
315 expansion (denoted as RR-2D), its predictions by far outperform its MLR-2D equivalent which now suffers from severe
316 overfitting (compare R^2 ~~scores values~~ in Fig. 3a and 3b). Noteworthy, with the increase of dimensionality in RR-2D, the
317 regularization strength now is adjusted to larger values starting from 10^3 to 10^9 with a factor of 1.42 incremental increase at
318 each step, which is much higher than the regularization strength set in RR with only local predictors. ~~Such~~ ~~Such~~ a large increase
319 ~~in~~ range is due to the consideration of adding ~~a~~ large number of meteorological predictors within the 2D domain, and it

320 ensures that the best solution with the most suitable regularization strength for each run can be well covered within this range.
 321 The overall R^2 [scores-values](#) for RR-2D [ranges-range](#) from 0.5 to 0.6 while R^2 in MLR-2D ranges from 0.3 to 0.4; MLR-2D is
 322 overall worse than MLR with only local meteorological predictors in terms of R^2 . It is well-known that RFR may not be as
 323 effective at handling multi-collinearity in very high dimensional settings as RR (e.g., Dormann et al., 2013) and its training
 324 time also increases exponentially with the number of predictors. We thus only ran RFR with 2D expansion (denoted as RFR-
 325 2D) for the southern Chinese PRD region, where we found a particularly large R^2 -[score-value](#) improvement after including
 326 non-local predictors in RR-2D ($R^2=0.60$) as compared to local RR ($R^2=0.47$), and even non-linear local RFR ($R^2=0.53$). These
 327 results highlight the apparent importance of large-scale meteorological phenomena in this region. However, we find that RFR-
 328 2D improves the average R^2 [score-value](#) (0.57) relative to RR and RFR with only local predictors, but does not perform better
 329 than RR-2D.



330
 331 **Figure 3** Coefficient of determination (R^2) between deseasonalized observational MDA8 ozone and deseasonalized predicted values
 332 of MDA8 ozone in ridge regression (RR) with 2D expansion (a) and MLR with 2D expansion (b).

333 For clarity, Table 2 summarizes the averaged R^2 in each region by all machine learning methods including RFR, RR,
 334 MLR, stepwise MLR, RR-2D, MLR-2D and RFR-2D. In summary, RFR and RR-2D are overall the two machine learning
 335 algorithms with [the](#) highest R^2 in these four regions, while MLR and RR are equivalent.

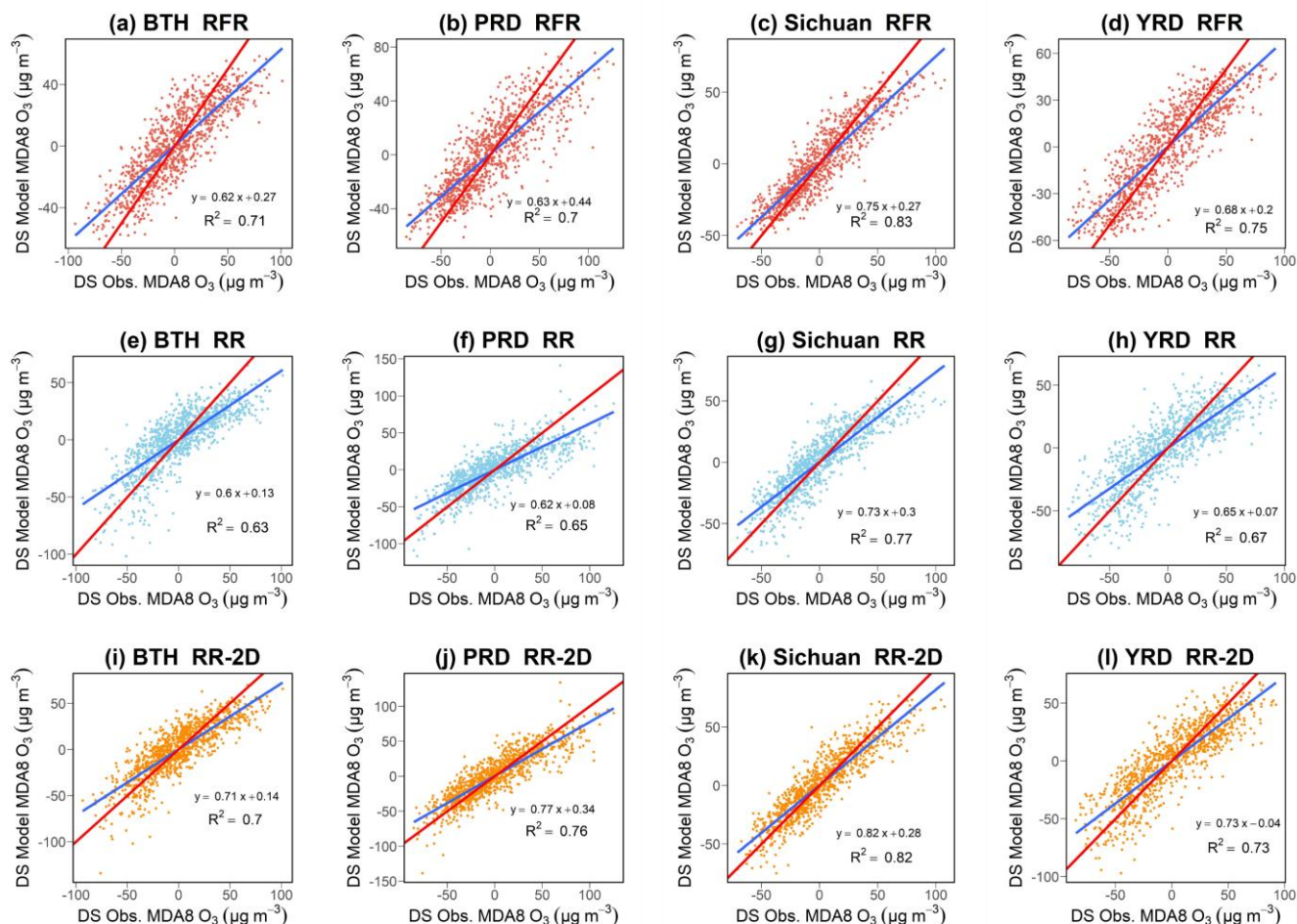
336 **Table 2.** Averaged R^2 in the four regions by different machine learning algorithms, namely RFR, RR, MLR and stepwise MLR with
 337 only local meteorological predictors, RR-2D, MLR-2D with additional two-dimensional (2D) non-local meteorological variables and
 338 RFR-2D which is only conducted for PRD region. In general, with only local meteorological variables, RFR performs the best with
 339 [the](#) highest averaged R^2 in four regions. RR-2D and RFR-2D show improvement over [the](#) PRD region compared to RFR.

Method	BTH	YRD	PRD	Sichuan
RFR	0.46	0.56	0.53	0.57
RR	0.41	0.48	0.47	0.53
MLR	0.41	0.48	0.47	0.53
stepwise MLR	0.39	0.45	0.43	0.52
RR-2D	0.47	0.54	0.60	0.58
MLR-2D	0.31	0.35	0.42	0.43
RFR-2D	-	-	0.57	-

340 3.3 Regionally averaged prediction skill

341 In order to assess the performance of the algorithms in modelling [the](#) regional average ozone, we further compared our
342 regionally-averaged machine learning predictions by RFR, RR and RR-2D against observations for each of the four selected
343 regions in China (Fig. 4), whereas previously we compared regional averages based on predictions for individual grid points
344 whose R^2 ~~scores-values~~ were subsequently averaged within each region. For this purpose, we averaged all $0.25^\circ \times 0.25^\circ$ grid
345 point observations and model results within each region first and then compared the resulting time series for each test dataset
346 directly. The results ~~of regional averaged predictions and observations~~ for each region are shown in Figure 4, where the goal
347 for the predictions is to fall as close as possible ~~onto to~~ the 1:1-line, in combination with a high R^2 -~~score-value~~ (~~coefficient of~~
348 ~~determination square of Pearson correlation, R~~). With only local meteorological predictors, RFR still outperforms RR
349 regarding both ~~the coefficient of determination (R^2 , same calculation method as above)~~ and slope (closer to 1) in all four
350 regions. This can likely be attributed to the ability of RFR to capture non-linearity as well.

351 Using this calculation method, [the](#) regional R^2 [values](#) are much higher; for RFR, regional R^2 in BTH, YRD, PRD and
352 Sichuan Basin ~~is~~[are](#) 0.71, 0.75, 0.7 and 0.83. ~~The higher values can be partially explained by the fact that, since each individual~~
353 ~~grid points is~~[are](#) more prone to the effect of local emissions and related local uncertainties, ~~where~~-as [larger](#) regional averages
354 can ~~factor smooth~~ out ~~some of these~~ local effects (~~i.e., emissions and uncertainties~~) to some extent. For instance, stations that
355 are located relatively close to [an](#) emission source may be more influenced by [the](#) NO_x -titration effect which may lower ozone
356 [level-levels](#) (Sillman, 1999). This effect can be more significant in some urban areas (Li et al., 2017) or stations affected by
357 fresh [emission-emissions](#) of NO_x from power plants (X. Zhang et al., 2021). ~~On the other hand, a~~Nearby emission of
358 precursors may also be the dominant factor in driving ozone [changes](#) in regular weather [condition-conditions](#). ~~Given both of~~
359 ~~these effects, o~~Ozone production in these stations may be less sensitive to meteorological drivers but more influenced by local
360 emissions.



361

362 **Figure 4 (a)-(d) Comparison of regional averages of deseasonalized MDA8 ozone between model predictions and observations for**
 363 **RFR, (e)-(h) RR and (i)-(l) RR-2D. Linear fits between predicted and observed data are indicated by blue lines; red lines are the**
 364 **ideal 1:1 lines. The values for both models and observations are averaged over all ERA grid points in each region. Each graph**
 365 **contains information of the linear regression with slope and R^2 score value (coefficient of determination, i.e., square of Pearson**
 366 **correlation, R .**

367 In summary, all ~~three~~ machine learning methods show clear-high skill in modelling meteorologically driven ozone
 368 variability ~~driven by meteorological variables~~. However, similar to results by Han et al. (2020), all linear fits of predicted
 369 versus observed ozone values in all regions for both RFR and RR have slopes lower than 1, suggesting a systemic
 370 underprediction of ozone for the highest observed ozone levels (higher than the deseasonalized zero mean) and overpredictions
 371 of ozone for low ozone pollution regimes (lower than the deseasonalized zero mean). As previously mentioned, such a
 372 mismatch may - at least to a degree - arise from non-meteorological factors such as the effect of precursor emissions, which
 373 are not taken into account here ~~given the assumption that the factors of that certain but not all emissions are not fully~~ are related
 374 to the meteorological factors. Although regionally averaged prediction skill is less affected by local emissions, it will not be
 375 completely free from such effects. ~~However, t~~ The increase of the magnitude of the slopes in RR-2D (~~with~~ closer to 1) also

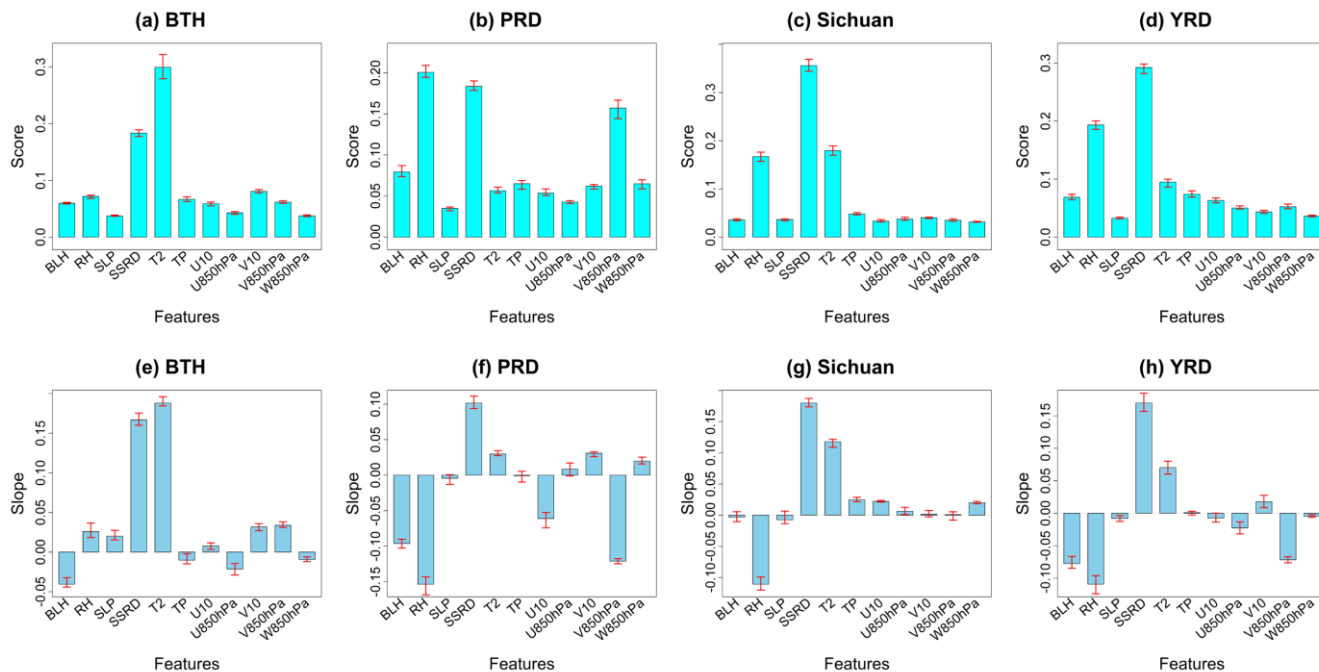
376 suggests that considering non-local meteorological variables may help improve the performance of ozone pollution controlling
377 factor analyses, even if non-linearity is not intrinsically taken into account.

378 3.4 Quantifying the importance of meteorological predictors

379 We next aim to quantify how important each local meteorological predictor is for ozone pollution across China. For RR,
380 we use the regression slope as a standard metric to measure how important of each the meteorological predictor on ozone
381 pollution. A large positive value for the slope (regression coefficient) of a meteorological predictor indicates that the predictor
382 has a strong positive effect on ozone levels and vice versa. Since each set of ~~the~~ 4-year training data is learned from
383 independently, we will show averaged results. For RFR, we measure each predictor's importance through Gini importance
384 (see Sect. 2.5). The highest absolute value for both the RR slope or RFR Gini importance is interpreted as the most important
385 meteorological driver variable identified through our data-driven learning procedure. Note that Gini importance only allows
386 to measure relative influences of predictor variables on ozone variability, but not the sign of the influence, i.e., a high value of
387 Gini importance score is not able to determine whether the predictor has a positive or negative effect on ozone.

388 The Gini importance scores estimated by RFR and the slopes learned by RR for each region are shown in Fig. 5. Both
389 Gini importance scores and slopes are initially estimated for every ERA5 grid location within each region and then averaged
390 across the entire region and across all five learned regression functions.

391



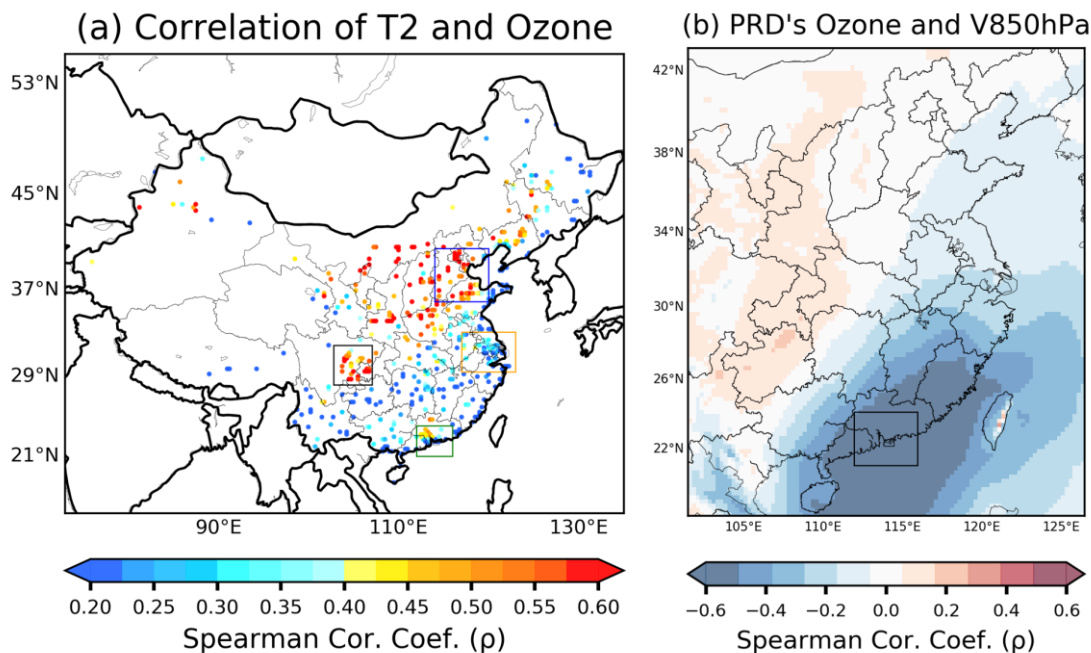
392

393 **Figure 5 (a)-(d) Average Gini feature importance scores of each meteorological variable for RFR in each region. (e)-(h) Average**
394 **slopes of each meteorological variable for ~~ridge regressions~~RR in each region. The red bars indicate the range of importance**
395 **scores/slopes found across the five regression models learned to predict the left-out test years.**

396 In general, both RFR and RR show good agreement in terms of identifying the dominant meteorological drivers for each
397 region. ~~Temperature~~The temperature at 2 m is found to be the most important meteorological driver for ozone in BTH,
398 followed by surface solar downward radiation, albeit the relative difference between these two variables differs more clearly
399 for RFR, which might be caused by non-linearity in the ozone-temperature relationship (Supplementary Fig. S5). Temperature
400 was also identified as the most important meteorological variable in BTH by Li et al. (2019a) using MLR. Moreover, a more
401 pronounced positive correlation between daily maximum temperature and MDA8 ozone is found in northern regions of China
402 (Fig. 6a), which is consistent with the findings of these two machine learning algorithms. ~~WithAs temperature beingis~~
403 ~~identified as the key meteorological factor in BTH,~~a more severe ozone pollution with increasing in higher temperature is
404 ~~expected since itand may be elevated by the~~caused by increased rates of chemical kinetics for ozone's production (e.g., Lu et
405 al., 2019a), the contribution of biogenic emissions (e.g., Ma et al., 2019) and anthropogenic emissions such as solvent
406 evaporation which may be intensified in hot weather (e.g., Song et al., 2019; Qi et al., 2017). ~~Biogenic emissions can be~~
407 ~~intensified during heatwaves in BTH, leading increased ozone (Ma et al., 2019).~~Additionally, high temperature conditions
408 ~~may also lead to the intensification of certain anthropogenic emissions such as solvent evaporation. A detailed emission~~
409 ~~inventory in 2013 for BTH shows that solvent use makes the highest contribution to NMVOC emissions at 46.7% in the~~
410 ~~industry sector (Qi et al., 2017). Song et al. (2019) conducted a one year observation (from April 2016 to March 2017) of~~
411 ~~VOCs at an urban site in BTH and found that biogenic emissions and solvent use can make major contribution to ozone~~
412 ~~formation, and the concentrations of the reactive VOCs species derived from these sources are found to have a positive~~
413 ~~correlation with temperature. In summary, with higher temperature, biogenic emissions and solvent evaporation may be more~~
414 ~~intense, which may be one of the underlying causes for elevated ozone pollution in BTH with higher temperatures.~~

415 For both YRD and Sichuan, surface solar radiation is most important determinant of ozone variations, with RR slopes
416 again indicating the expected positive relationship between sunny, clear-sky days and high ozone pollution. ~~Furthermore,~~
417 ~~surface s~~Solar radiation is ~~also~~ found to be ~~central-important~~ in BTH, PRD by RFR and RR, ~~suggesting its consistent~~
418 ~~importance across China. Given that Li et al. (2019a; 2020) and Han et al. (2020) did not consider this meteorological variable~~
419 ~~in their analyses, we recommend that -it could be used more generally in the future~~The importance of solar radiation should
420 ~~be given more consideration in assessing the effect of meteorological drivers on ozone pollution.~~ High solar radiation
421 stimulates the photochemical environment, which has been suggested as one of the key mechanisms in YRD by Pu et al. (2017).
422 From a large-scale meteorological point of view, such clear-sky conditions in YRD that may enhance severe ozone pollution
423 in this region ~~may be are~~modulated by the western Pacific subtropical high (WPSH) (Shu et al., 2016; Chang et al., 2019; Shu
424 et al., 2020). In the Sichuan Basin, with complex terrain that can complicate atmospheric circulation, ozone pollution is often
425 associated with the occurrence of high-pressure systems associated with clear-sky conditions and high temperatures (Ning et
426 al., 2020), which is also identified by both RFR and RR.

427 A distinct difference in the weather-ozone coupling relationships is found for PRD, where relative humidity is the
428 dominant meteorological driver. Specifically, a negative slope of RH in RR suggests that drier conditions are strongly favorable
429 for peak ozone concentrations in PRD. As one of many possible effects of humidity, ozone may be more destroyed through
430 the photolysis reaction of $O_3 + hv \rightarrow O(^1D) + O_2$ as $O(^1D)$ can subsequently react with H_2O , forming OH through reaction of
431 $O(^1D) + H_2O \rightarrow 2OH$, which will be enhanced in environments with high humidity (Wang et al., 2013; Young et al., 2013).
432 In addition, despite more OH may be available given high humidity, OH can react with NO_2 , forming HNO_3 in highly NO_x -
433 polluted regions, which ultimately ~~leading-leads~~ to less efficient O_3 formation by competing with the oxidation of VOC and
434 CO with OH (Lu et al., 2019a). The negative correlation between humidity and ozone in the PRD region has been identified
435 by previous studies (W. Zhang et al., 2021; Yang et al., 2021; Hua et al., 2008), and the high humidity environment in southern
436 China may be the result of moisture marine air masses transported from tropical region, the South China Sea and western
437 Pacific (W. Zhang et al., 2021; Ding and Chae, 2005). For a non-linear learning framework using RFR, the second most
438 important meteorological driver in PRD is again the level of surface solar radiation. Interestingly, meridional wind at 850 hPa
439 is key to ozone occurrence in PRD, and it is negatively correlated with average MDA8 ozone. More ~~generally~~specifically, the
440 regional average of MDA8 ozone in PRD is negatively correlated with the meridional wind at 850 hPa from the South China
441 Sea (Fig. 6b), indicating strong marine air inflow may have a significant cleaning and dispersion effect on ~~PRD~~-ozone and its
442 precursors in PRD. Furthermore, the negative correlation also expands to the northeast areas ~~to~~of the PRD, suggesting lower
443 ozone in PRD given strong southerly wind in these areas, which may hinder the transport of ozone and its precursors to PRD.
444 This finding is consistent with the backward trajectories and numerical modelling analysis by Qu et al. (2021).

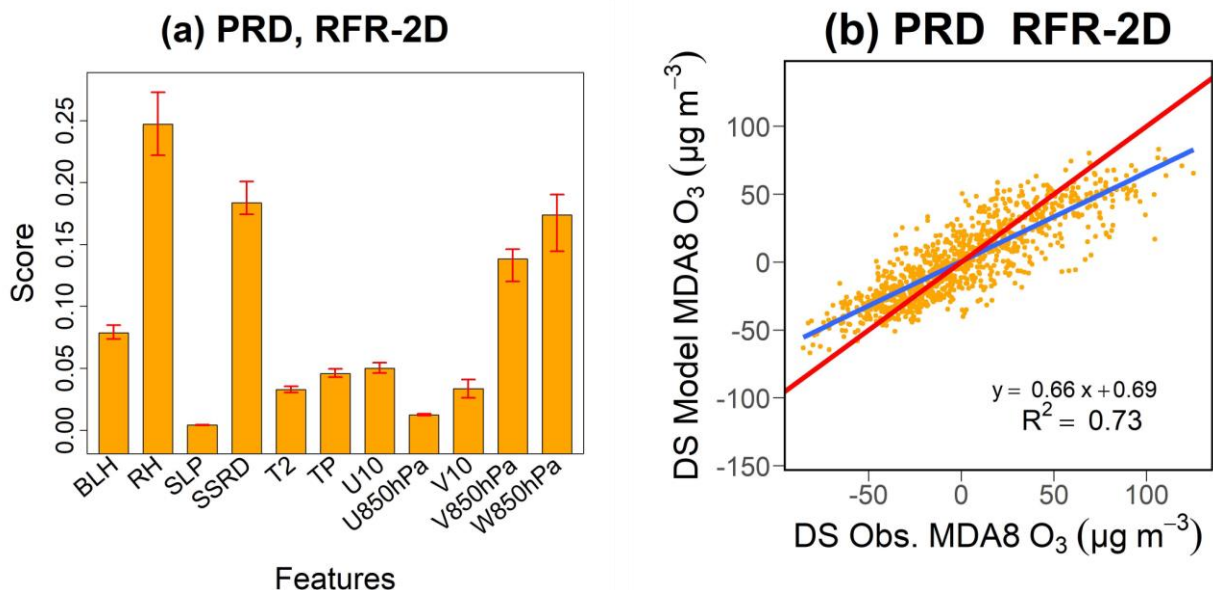


445

446 **Figure. 6 (a) Spearman correlation between daytime (06:00 to 18:00) averaged temperature at 2 m and MDA8 ozone from 2015 to**
447 **2019 from April to October. (b) Correlation coefficients between the regional average of MDA8 ozone in PRD and the daytime (06:00**
448 **to 12:00) meridional wind at 850 hPa at each ERA5 grid point from April to October of 2015 to 2019. A positive value of meridional**
449 **wind indicates southerly wind.**

450 Additionally, previous studies (Jiang et al., 2015; Z. Chen et al., 2021; Qu et al., 2021; Wei et al., 2016) also indicate the
451 importance of vertical downward transport of ozone in southern region of China due to the impact of typhoons. The effect of
452 such a downward transport may not be well captured by regressions with only local meteorological predictors as it is a larger-
453 scale meteorological phenomenon. The geographical location and the intensity of typhoons can modulate the level of ozone in
454 PRD; when typhoons are located relatively far away from PRD during their development period, ozone can be elevated by
455 downward movement of air masses, atmospheric stagnation and lower planetary boundary layer height (Z. Chen et al., 2021),
456 leading to suppressed dispersion of ozone and its precursors before typhoon landing (Jiang et al., 2015; Z. Chen et al.,
457 2021). ~~To illustrate the importance of such larger scale meteorological effects on ozone pollution in PRD,~~ we refer
458 back to our two-dimensional (2D) approach for RFR in the PRD region first introduced and described in Sect. 3.2. We show
459 the Gini feature importance scores for this 2D domain approach in Fig. 7(a). Since we have multiple values of the feature
460 importance for each meteorological variable in this set-up (i.e., one for each grid point in the 2D predictor domain), we sum
461 up Gini scores for all grid points within the expanded domain for each meteorological variable; and this summed value is
462 denoted as the importance for that particular meteorological variable. As illustrated in Fig. 7 (a), the relative feature importance
463 of vertical velocity at 850hPa (W_w850hPa) increases compared to RFR using only local predictors (see Fig. 5b), likely
464 reflecting the larger-scale influences of downward transport of air masses in the PRD region. Other key meteorological drivers
465 (RH, surface solar radiation and meridional wind at 850 hPa) remain in a similar order to what was identified by purely local
466 regressions. The model performance is slightly improved by adding the 2D information with an increase of R^2 to 0.73 (from
467 0.70) in comparison to the original RFR without 2D expansion. However, we note that the R^2 in RFR-2D for PRD region (Fig.
468 7b) is 0.73 which is slightly less than the R^2 using RR-2D (0.76), and the slope of the linear fit between the predictions from
469 RR-2D and the observations is closer to 1 (Fig. 4j) when compared in contrast to RFR-2D (Fig. 7b). The higher R^2 from RR-
470 2D may be attributed to RR's ability to ~~ability-~~ extrapolate ~~extrapolating~~ the extreme high/low anomalies of observed ozone,
471 while the prediction range of RFR-2D is more- constrained ~~subjected by~~ to the range of anomalies from the training data. For
472 example, RR-2D can better predict the extreme low anomaly of observed ozone on 2015-Oct-4 (Fig. S6). Nevertheless, there
473 could be a trade-off in the feature of extrapolation of RR. For instance, in terms of slope, the seemingly better slope (i.e., closer
474 to 1) from RR-2D (Fig. 4j) may be partly due to its limitation of over- and underpredicting some extreme high/low anomalies,
475 which can be illustrated by outliers from linear fit in Fig. 4j. This can be exemplified by the overprediction of ozone anomaly
476 on 2015-Apr-14 by RR-2D (also see Fig. S6). Such ~~an~~ effects of over- or underpredictions under extrapolation can to a degree
477 compensate the bias in the predicted vs. observed slope, bringing it closer to the 1:1 line. ~~there appears to be a trade off~~
478 between the inclusion of non-linear relationships using RFR and collinearity or overfitting in high dimensions. Indeed, we find
479 that the R^2 in RFR 2D for PRD region (see Fig. 7b) is still slightly less than the R^2 using RR 2D (0.76) and the predictions
480 from RR 2D are closer to observations with less ~~fewer~~ deviations at both high and low ozone value predictions (see Fig. 4j),

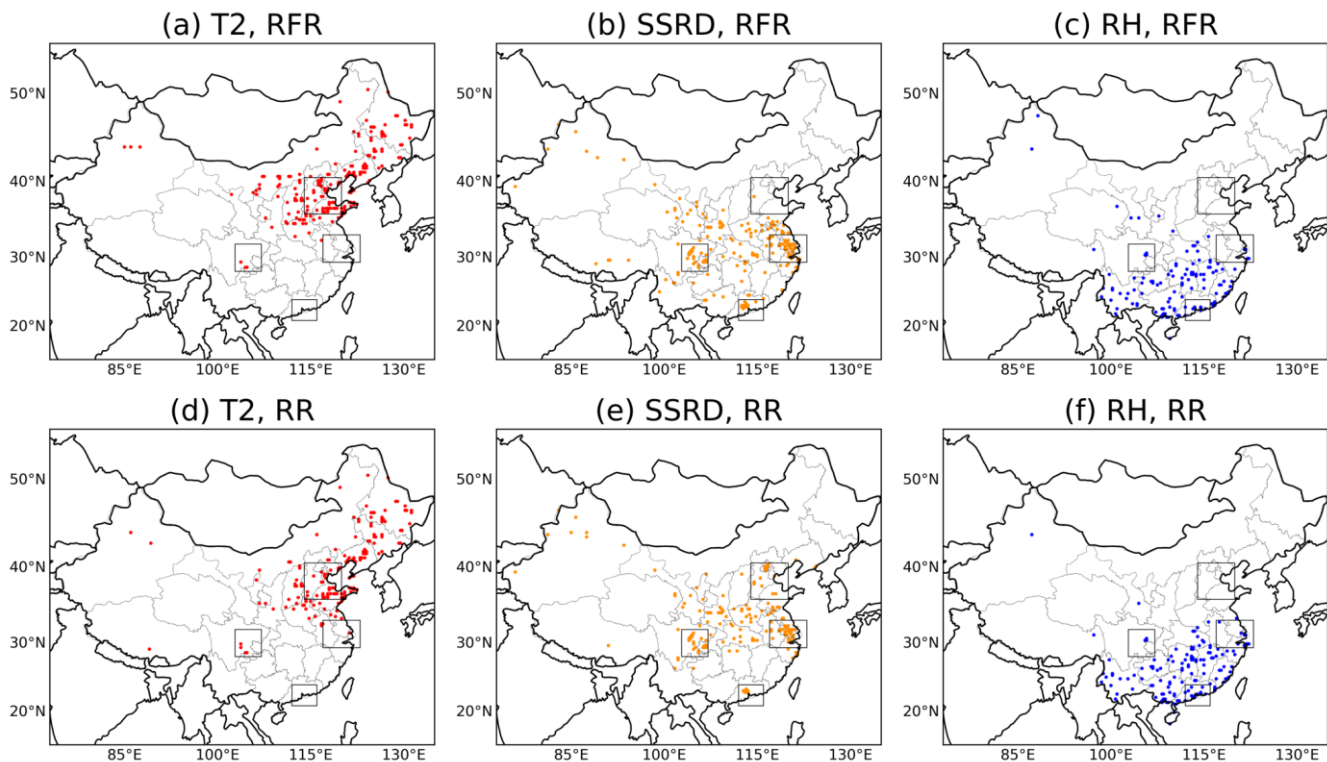
481 suggesting that RR is better at handling the dimensionality increase of predictors, which now slightly outweighs the importance
482 of non-linearity in high dimensions.



483

484 **Figure 7.** (a) Average PRD Gini feature importance score of each meteorological variable if each the RFR regressions includes non-
485 local predictors within a 7.5° longitude × 7.5° latitude domain around the predicted grid point grid; the bar representations are
486 consistent with Figure 5. (b) Linear fit between model-RFR-2D predictions and observations in PRD (using this 2D approach is
487 drawn in blue line). The red line equals the ideal 1:1 relationship line.

488 Across China, we found that there is a consistency in the identification of the three most important meteorological drivers
489 by RFR and RR: temperature, surface solar radiation and RH (are the three most commonly found most important
490 meteorological drivers across China, and the spatial distributions of these drivers are presented in Fig.8). Overall, there is a
491 distinctive distribution pattern of the 3 major meteorological drivers in China. Temperature-The temperature at 2 m is dominant
492 over northeast China, covering BTH and expand-expanding to the norther-northern region of China. Most areas in the mid-
493 latitude regions of China, including East China (e.g., YRD) and the Sichuan Basin, show surface solar radiation as the main
494 meteorological driver for ozone, suggesting the necessity of including this variable for analyses. The dominance of surface
495 solar radiation gradually expands northward and southward from this region while being overtaken by temperature in the north
496 and relative humidity in the south. Ozone in southern China is primarily driven by relative humidity. Such a distinctive spatial
497 distribution of meteorological drivers may be related to the characteristics of regional climatology. For instance, as previously
498 described above, regions in the-southern China such as PRD are more-particularly influenced by the-moisturevariations in
499 incoming moist air masses, leading to the importance of humidity surpassing temperature and surface solar radiation. While
500 the relative-relatively drier northern regions do not have such a changeable humidity conditions, making temperature and
501 surface solar radiation the key meteorological factors driving ozone.



502

503 **Figure 8 (a)-(c) Most important meteorological drivers at each grid location from April to October of 2015 to 2019 as identified by**
 504 **Gini importance using RFR. (d)-(f) The same but using absolute magnitudes for the slopes of RR. Variables as labelled. Relative**
 505 **humidity (RH) dominates in the South and South-East, surface solar downward radiation (SSRD) primarily in the Central China**
 506 **and Eastern China, and temperature at 2 m (T2) in the North and North-East China.**

507 3.5 Anthropogenic and meteorological contributions to surface ozone trends from 2015 to 2019

508 Finally, we explore how our new ~~machine learning~~ approach could be used to study the quantitative influence of
 509 meteorology on historical ozone variability and trends in China. To facilitate a comparison to previous work, we use a similar
 510 method as Li et al. (2020) to establish estimates for observed surface ozone trends in China. We note that our exercise is
 511 somewhat limited by the slightly shorter period considered here, i.e., from 2015 to 2019, instead of starting from earlier years.
 512 Given this very short period, we are aware that any long-term trend analysis is explorative and has to be interpreted carefully,
 513 as will also become evident from low statistical significance in many detected trends. We nevertheless attempt such an analysis
 514 to demonstrate how our method can be used in such contexts and to also evaluate if any statistically significant trends are
 515 robust after accounting for meteorological influences. ~~After all, as we have demonstrated above, we can quantify such~~
 516 ~~influences with greater skill than using simple MLR methods applied previously.~~

517 For trend analyses, we first convert MDA8 ozone concentrations from mass concentrations ($\mu\text{g m}^{-3}$) to volume mixing
 518 ratios (ppbv). We then average MDA8 ozone over April to October or summertime for each year for both observational data
 519 and model results predicted by our three ~~best performing machine learning-based controlling factor~~ regressions (RFR, RR and

520 RR-2D) ~~and MLR algorithm~~. Both stepwise MLR and MLR-2D are not included in the trend analyses here since these two
 521 ~~algorithms show~~ have overall weak performances in modelling ozone (see Table 2). The predictions can be considered as a
 522 quantitative estimate for the influence of meteorology on the ozone record during the study period. The residual (true ozone
 523 signal minus meteorological predictions) will for example be mainly reflective of anthropogenic contributions but will also
 524 inevitably contain some uncertainties related to the accuracy of the ~~machine learning algorithms~~ controlling factor regressions
 525 ~~in modelling ozone~~.

526 Table 3 summarizes the regionally averaged observed trends from 2015 to 2019, which is estimated by ordinary linear
 527 regression in the four regions. We additionally list our meteorologically estimated trends and the residual trends. Overall, the
 528 three machine learning methods ~~and MLR~~ provide ~~relatively very~~ similar estimates of meteorologically driven trends in BTH,
 529 YRD and Sichuan Basin, while we find indications that the meteorologically driven trend in PRD may be underestimated by
 530 only using local meteorological factors; using RR-2D we estimate a meteorologically driven trend of 0.84 ppbv a⁻¹ during
 531 April to October from 2015 to 2019, while RFR, ~~and RR~~ ~~and MLR~~ with only local meteorological predictors provide estimates
 532 of 0.1 ppbv a⁻¹, ~~and~~ 0.003 ppbv a⁻¹ ~~and 0.04 ppbv a⁻¹~~, respectively. Given the better prediction skill in RR-2D for this region
 533 (see Table 2 and Fig. 4), this further suggests the importance of spatial meteorological phenomena for ozone trend attribution
 534 exercises in the PRD region.

535 In terms of the raw observed trends, both BTH and PRD show significant increases in ozone pollution ($p < 0.05$) ~~during~~
 536 ~~from~~ April to October ~~for from~~ 2015 to 2019. We note that the observed trend in PRD is only significant if the months ~~from~~
 537 April to October are considered, whereas there is no significant trend ($p = 0.93$) if only examining months in summertime (JJA).
 538 This may be attributed to the ozone's seasonality in PRD where ~~the~~ highest ozone pollution occurs during autumn and the
 539 particularly high ozone anomaly during September and October in 2019 (Fig. S7**6**b). We underline that anthropogenic
 540 contribution (i.e., the residual) may be overestimated in PRD if only local meteorological factors are considered, given that
 541 ~~both~~ residuals of RFR, ~~and RR~~ ~~and MLR~~ increase compared to RR-2D. For BTH, the positive ozone trend is found to be ~~higher~~
 542 ~~more significant~~ during summertime at 3.20 ppbv a⁻¹ ($p = 0.05$) than if the whole April to October period (2.53 ppbv a⁻¹, $p < 0.05$)
 543 is considered. Moreover, estimated by RFR, the meteorologically driven trend in BTH is also higher at 0.74 ppbv a⁻¹ ($p < 0.1$)
 544 during summertime than if the whole April to October period is considered (0.45 ppbv a⁻¹; $p = 0.14$). The April-to-October
 545 residual trends in BTH estimated by all ~~three-four~~ algorithms are all greater than 2 ppbv a⁻¹ ($p < 0.1$), indicating an elevated
 546 importance of anthropogenic drivers in BTH. There are no significant observed trends in YRD and Sichuan. However,
 547 meteorological factors in both of these regions appear to ~~make-have~~ a stronger influence ~~on the trends of ozone~~ according to
 548 ~~these four algorithms~~ RFR, RR ~~and RR-2D~~. ~~In terms of regional averages,~~ ~~Additionally,~~ all ~~three-four~~ of the ~~machine learning~~
 549 ~~algorithms~~ ~~methods~~ also agree on meteorologically driven negative trends in Sichuan while positive trends are found for YRD.

550 **Table 3. Observational, meteorological and residual trends of regional averaged MDA8 ozone (ppbv a⁻¹) from 2015 to 2019 for both**
 551 **April to October and Northern Hemisphere summertime (June, July, August). Values within the brackets are the p values for each**
 552 **trend. Trends and p values are in bold given p values smaller than 0.1.**

2015-2019 Apr. to Oct.

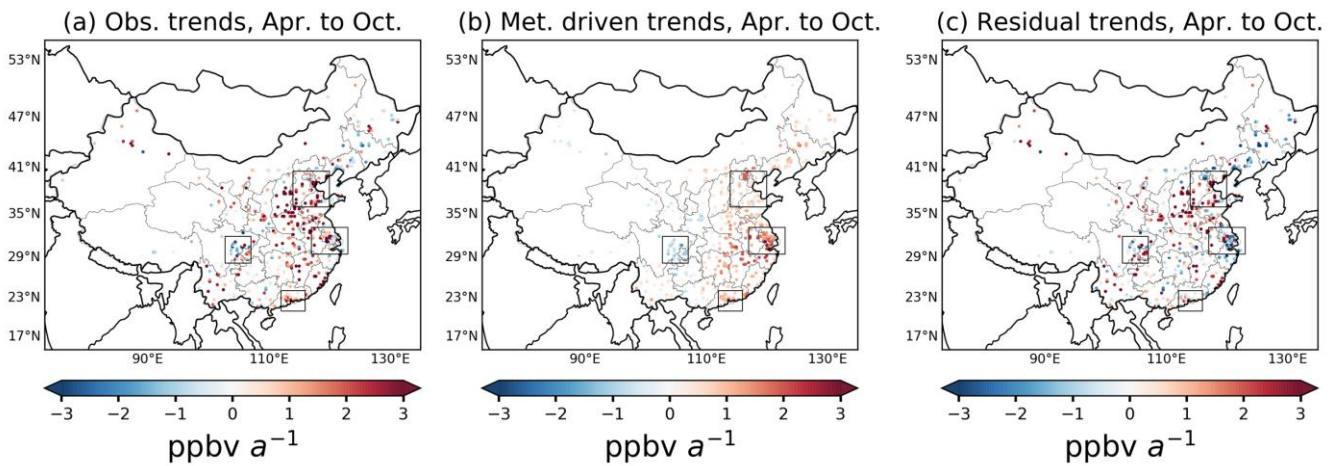
2015-2019 Summer

Method	Regions	Observed	Meteorological	Residual	Observed	Meteorological	Residual
RFR	BTH	2.53 (0.02)	0.45 (0.14)	2.08 (0.04)	3.2 (0.05)	0.74 (0.08)	2.46 (0.06)
	PRD	1.18 (0.02)	0.1 (0.88)	1.08 (0.08)	-0.12 (0.93)	-0.75 (0.14)	0.64 (0.58)
	Sichuan	-0.34 (0.57)	-0.75 (0.04)	0.42 (0.32)	0.01 (0.99)	-0.91 (0.34)	0.92 (0.11)
	YRD	0.87 (0.36)	1.38 (0.04)	-0.51 (0.48)	1.53 (0.15)	1.35 (0.07)	0.17 (0.81)
RR	BTH	2.53 (0.02)	0.37 (0.17)	2.17 (0.03)	3.2 (0.05)	0.54 (0.18)	2.66 (0.05)
	PRD	1.18 (0.02)	0.003 (0.997)	1.18 (0.09)	-0.12 (0.93)	-1.13 (0.11)	1.01 (0.39)
	Sichuan	-0.34 (0.57)	-0.84 (0.05)	0.51 (0.18)	0.01 (0.99)	-0.84 (0.4)	0.85 (0.06)
	YRD	0.87 (0.36)	1.41 (0.04)	-0.54 (0.43)	1.53 (0.15)	1.38 (0.09)	0.14 (0.86)
RR-2D	BTH	2.53 (0.02)	0.47 (0.35)	2.06 (0.09)	3.2 (0.05)	0.7 (0.33)	2.5 (0.11)
	PRD	1.18 (0.02)	0.84 (0.31)	0.34 (0.58)	-0.12 (0.93)	-0.33 (0.62)	0.21 (0.81)
	Sichuan	-0.34 (0.57)	-0.86 (0.02)	0.52 (0.25)	0.01 (0.99)	-0.68 (0.46)	0.69 (0.21)
	YRD	0.87 (0.36)	1.45 (0.08)	-0.58 (0.47)	1.53 (0.15)	1.63 (0.02)	-0.10 (0.91)
MLR	BTH	2.53 (0.02)	0.37 (0.19)	2.16 (0.02)	3.2 (0.05)	0.55 (0.19)	2.65 (0.05)
	PRD	1.18 (0.02)	0.04 (0.96)	1.14 (0.12)	-0.12 (0.93)	-1.1 (0.14)	0.98 (0.4)
	Sichuan	-0.34 (0.57)	-0.86 (0.05)	0.53 (0.16)	0.01 (0.99)	-0.86 (0.4)	0.87 (0.05)
	YRD	0.87 (0.36)	1.42 (0.05)	-0.55 (0.43)	1.53 (0.15)	1.42 (0.08)	0.1 (0.9)

553

554 Finally, we aim to calculate trends on a ERA5 grid-by-grid point basis. Although both RFR, RR and RR-2D ~~all~~ show
555 significant overall better skill in modelling ozone across China, RR-2D exhibited particularly increased predictive skill in
556 southern China. Therefore, for assessing meteorologically-driven trends of MDA8 ozone across all ERA5 grid locations in
557 China, we will only be examining the results for RR-2D. Fig. 9 shows trends during April to October from 2015 to 2019 across
558 China. Overall, the observed average trend across China is 1.1 ppbv a⁻¹. The meteorologically driven trend of RR-2D gives the
559 average at 0.5 ppbv a⁻¹ across China, which is around 45% of the total trend. From Fig. 9 (a), most regions in eastern China
560 show a positive trend and the magnitudes of increase are more apparent in areas within and nearby BTH, where the ozone
561 pollution increased at an average rate of 2.6 ppbv a⁻¹ across all grids within BTH. We find that the positive trend in those
562 particular regions may be less driven by meteorological factors but indeed might be the result of anthropogenic influences on
563 air pollution (e.g., Liu and Wang, 2020). In YRD, meteorologically driven positive trends are in general the highest in eastern
564 China (average at 1.47 ppbv a⁻¹ across all grids in YRD), which is close to the regionally averaged result by RR-2D (1.45 ppbv
565 a⁻¹, $p=0.08$) in Table 3. Observed trends in Sichuan are a mixture of both increases and decreases, but meteorologically driven
566 trends are all negative within this region. In PRD, meteorological factors likely played a more central role in driving the recent
567 positive trends in ozone pollution according to our analysis.

568



569

570 **Figure. 9 Trends of MDA8 ozone during April to October from 2015 to 2019.** (a) shows the observed trends. (b) shows the mean
 571 meteorologically driven trends of MDA8 ozone according to RR-2D. (c) shows the trends of residuals (approximating anthropogenic
 572 effects). The trends are estimated by the slopes of an ordinary linear regression fitting each year's April-October MDA8 average
 573 ozone values from 2015 to 2019.

574 4 Conclusion

575 Ozone pollution in China can be strongly influenced by meteorological conditions. This study examines the major
 576 meteorological drivers for ozone pollution across China during months with particularly high ozone pollution (i.e., April to
 577 October, from 2015 to 2019) using a controlling factor framework and two machine learning algorithms, namely random forest
 578 regression (RFR) and ridge regression (RR).

579 The results obtained with RFR and RR are also compared with conventional approaches i.e., multiple linear regression
 580 (MLR) and stepwise MLR, using consistent out-of-sample cross-validation methods. When considering local meteorological
 581 factors only, RFR outperforms the linear approaches RR and MLR, which in turn perform better than stepwise MLR that uses
 582 ~~the~~ only the three locally most significant meteorological factors. ~~In terms of fitness between predicted and observational~~
 583 ~~ozone, the better performance of RFR can be illustrated~~ is for example evident from ~~by~~ the overall increase ~~of~~ in predicted
 584 ~~versus observed coefficients of determination (R^2) ranging from 0.5 to 0.6, while most of R^2 of these as compared to 0.4 to 0.5~~
 585 ~~for the three linear regressions are within the range of 0.4 to 0.5. Stepwise MLR shows least ability for accurately modelling~~
 586 ~~ozone in contrast to the other algorithms, which can be illustrated by its attains the lowest averaged R^2 of all these methods~~
 587 ~~across China. Within the context of modelling by using only local meteorological predictors in the regressions, a~~ major
 588 advantage of RFR ~~, when compared to linear regressions,~~ is its ability to model non-linear relationships ~~between~~
 589 ~~meteorological variables and ozone~~ (e.g., often observed between temperature and ozone). In addition, we tested how the
 590 consideration of ~~larger-scale~~ larger-scale meteorological controlling factors improves our predictive performance. MLR
 591 noticeably suffers from the “curse of dimensionality” due to the large increase ~~of in~~ the number of predictors when we included
 592 additional meteorological information spanning a $7.5^\circ \times 7.5^\circ$ domain around the target grid point for ozone pollution ~~(since the~~

593 ~~majority of R^2 values of this approach fall to a lower range of 0.3 to 0.4~~. In contrast, RR can deal well with this increase in
594 the number of predictors subject to an objective cross-validation approach for its hyperparameter tuning. In particular, despite
595 not directly considering non-linearity, we find an improvement of model performance in RR with additional 2-dimensional
596 predictors, which even outperforms itself and RFR, with only local meteorological predictors especially particularly in
597 southern China, indicating the importance of considering a wider meteorological context in future controlling factor analyses
598 of this kind.

599 A key advantage of our approach is that both RFR and RR allow for a straightforward interpretation of the predictive
600 models (explainable machine learning). Reassuringly, we find a good agreement regarding the identification of the dominant
601 local meteorological drivers for each region. In general, ozone pollution in northern China such as in the Beijing-Tianjin-Hebei
602 (BTH) region is predominantly driven by temperature fluctuations while ozone in southern China like in Pearl River Delta
603 (PRD) region is particularly strongly controlled by humidity, possibly due to the important role of humid weather in preventing
604 significant ozone pollution episodes in this region, ~~while the effect of humidity is constrained in BTH probably because of the~~
605 ~~relatively drier condition in this region~~. Besides, we observe a strong influence in PRD of air exchange with pristine marine
606 regions, leading to a greater influence of large-scale wind directions, e.g., through the transport of clean marine air into the
607 region, or through air stagnation and ozone accumulation under large-scale sinking atmospheric motion. Surface solar radiation
608 plays a major role in general due to its importance ~~for in~~ setting the conditions for ozone photochemistry, which is particularly
609 dominant in the Yangtze River Delta (YRD) and Sichuan Basin. Our work thus highlights that surface solar radiation ~~might~~
610 be a key predictor to consider in future controlling factor analyses ~~in these two regions~~. In summary, hot, dry and sunny weather
611 tends to provide more favorable conditions for ozone pollution in China, which is not entirely unexpected but carries important
612 implications for future changes in air pollution under climate change, while simultaneously considering the pivotal role of
613 targeted emission control strategies on ozone precursors.

614 In terms of ozone trends, we find a linear MDA8 ozone increase of about 1.1 ppbv a⁻¹ on average during April to October
615 from 2015 to 2019 across China. Regionally, these trends can be more than twice as large as in BTH. The largest positive
616 trends may be mostly attributed to non-meteorological factors such as change changes in precursors² emissions. However,
617 meteorologically driven trends on average shows increases at 0.5 ppbv a⁻¹ across China, equalling almost 50% over the period
618 considered here, and it is thus estimated to be a more important factor, especially in southern China and the YRD region. The
619 importance of large-scale meteorological phenomena is highlighted in southern China as a higher averaged meteorological
620 contribution to the increase trend of ozone in PRD is estimated by RR with non-local meteorological predictors. ~~While the~~
621 ~~effect of m~~ Meteorology ~~might generally hinder~~ appears to have amplified negative ozone trends extreme ozone pollution in
622 the Sichuan Basin region during 2015-2019, implying that. However, it is recommended to maintain ~~as a negative~~
623 ~~meteorologically driven trend is estimated, it is still preferable to maintain~~ we conclude that maintaining continuous emission
624 control strategies in this region in order to counter the occurrence of is preferable are required given that an eventual return
625 towards in case of more the occurrence of more unfavorable weather conditions for ozone mitigation is likely.

626 **Data/Code availability**

627 The original air quality data including hourly and 8-hour rolling mean of ozone are available at <https://quotsoft.net/air/>
628 (Wang, X. L., 2021; last accessed: 13 July 2021). The ERA5 reanalysis product is available at
629 <https://cds.climate.copernicus.eu/> (last accessed: 11 November 2021). The codes for machine learning algorithms are available
630 from the corresponding author upon request.

631 **Author contribution**

632 P.N., X.W. and G.F. designed the study. X.W. performed the modelling and analysis of the data, supervised by P.N. and
633 G.F. X.W. wrote the paper with input and revision from P.N. and G.F.

634 **Competing interests**

635 The authors declare that they have no conflict of interest.

636 **References**

- 637 Archibald, A. T., Turnock, S. T., Griffiths, P. T., Cox, T., Derwent, R. G., Knote, C., and Shin, M.: On the changes in
638 surface ozone over the twenty-first century: sensitivity to changes in surface temperature and chemical mechanisms:
639 21st century changes in surface ozone, *Philos. Trans. R. Soc. A Math. Phys. Eng. Sci.*, 378,
640 <https://doi.org/10.1098/rsta.2019.0329>, 2020.
- 641 Bishop, C. M.: *Pattern recognition and machine learning*, Springer Science+Business Media, Singapore, 2006.
- 642 Breiman, L.: Random Forests, *Mach. Learn.*, <https://doi.org/10.1023/A:1010933404324>, 2001.
- 643 Ceppi, P. and Nowack, P.: Observational evidence that cloud feedback amplifies global warming, *Proc. Natl. Acad. Sci. U.*
644 *S. A.*, 118, 1–7, <https://doi.org/10.1073/pnas.2026290118>, 2021.
- 645 Chang, L., Xu, J., Tie, X., and Gao, W.: The impact of Climate Change on the Western Pacific Subtropical High and the
646 related ozone pollution in Shanghai, China, *Sci. Rep.*, 9, 1–12, <https://doi.org/10.1038/s41598-019-53103-7>, 2019.
- 647 Chen, X., Jiang, Z., Shen, Y., Li, R., Fu, Y., Liu, J., Han, H., Liao, H., Cheng, X., Jones, D. B. A., Worden, H., and Abad, G.
648 G.: Chinese Regulations Are Working—Why Is Surface Ozone Over Industrialized Areas Still High? Applying Lessons
649 From Northeast US Air Quality Evolution, *Geophys. Res. Lett.*, 48, <https://doi.org/10.1029/2021GL092816>, 2021.
- 650 Chen, Z., Liu, J., Cheng, X., Yang, M., and Wang, H.: Positive and negative influences of typhoons on tropospheric ozone
651 over southern China, *Atmos. Chem. Phys.*, 21, 16911–16923, <https://doi.org/10.5194/acp-21-16911-2021>, 2021.
- 652 Chinese State Council: Action Plan on Air Pollution Prevention and Control (in Chinese), available at:
653 http://www.gov.cn/zwgc/2013-09/12/content_2486773.htm (last access: 24 November 2021), 2013.

654 Ding, Y. and Chan, J. C. L.: The East Asian summer monsoon: An overview, *Meteorol. Atmos. Phys.*, 89, 117–142,
655 <https://doi.org/10.1007/s00703-005-0125-z>, 2005.

656 Doherty, R. M., Wild, O., Shindell, D. T., Zeng, G., MacKenzie, I. A., Collins, W. J., Fiore, A. M., Stevenson, D. S.,
657 Dentener, F. J., Schultz, M. G., Hess, P., Derwent, R. G., and Keating, T. J.: Impacts of climate change on surface
658 ozone and intercontinental ozone pollution: A multi-model study, *J. Geophys. Res. Atmos.*, 118, 3744–3763,
659 <https://doi.org/10.1002/jgrd.50266>, 2013.

660 Dormann, C. F., Elith, J., Bacher, S., Buchmann, C., Carl, G., Carré, G., Marquéz, J. R. G., Gruber, B., Lafourcade, B.,
661 Leitão, P. J., Münkemüller, T., McClean, C., Osborne, P. E., Reineking, B., Schröder, B., Skidmore, A. K., Zurell, D.,
662 and Lautenbach, S.: Collinearity: A review of methods to deal with it and a simulation study evaluating their
663 performance, *Ecography.*, 36, 27–46, <https://doi.org/10.1111/j.1600-0587.2012.07348.x>, 2013.

664 Finlayson-Pitts, B. and Pitts, J.: *Chemistry of the upper and lower atmosphere*, Academic Press, San Diego, 2000.

665 Gao, M., Gao, J., Zhu, B., Kumar, R., Lu, X., Song, S., Zhang, Y., Jia, B., Wang, P., Beig, G., Hu, J., Ying, Q., Zhang, H.,
666 Sherman, P., and B. McElroy, M.: Ozone pollution over china and india: Seasonality and sources, *Atmos. Chem. Phys.*,
667 20, 4399–4414, <https://doi.org/10.5194/acp-20-4399-2020>, 2020.

668 Grange, S. K., Carslaw, D. C., Lewis, A. C., Boleti, E., and Hueglin, C.: Random forest meteorological normalisation
669 models for Swiss PM10 trend analysis, *Atmos. Chem. Phys.*, 18, 6223–6239, [https://doi.org/10.5194/acp-18-6223-](https://doi.org/10.5194/acp-18-6223-2018)
670 2018, 2018.

671 Gu, Y., Li, K., Xu, J., Liao, H., and Zhou, G.: Observed dependence of surface ozone on increasing temperature in Shanghai,
672 China, *Atmos. Environ.*, 221, <https://doi.org/10.1016/j.atmosenv.2019.117108>, 2020.

673 Guenther, A. B., Zimmerman, P. R., Harley, P. C., Monson, R. K., and Fall, R.: Isoprene and monoterpene emission rate
674 variability: model evaluations and sensitivity analyses, *J. Geophys. Res.*, 98, <https://doi.org/10.1029/93jd00527>, 1993.

675 Han, H., Liu, J., Shu, L., Wang, T., and Yuan, H.: Local and synoptic meteorological influences on daily variability in
676 summertime surface ozone in eastern China, *Atmos. Chem. Phys.*, 20, 203–222, [https://doi.org/10.5194/acp-20-203-](https://doi.org/10.5194/acp-20-203-2020)
677 2020, 2020.

678 Hersbach, H., Bell, B., Berrisford, P., Hirahara, S., Horányi, A., Muñoz-Sabater, J., Nicolas, J., Peubey, C., Radu, R.,
679 Schepers, D., Simmons, A., Soci, C., Abdalla, S., Abellan, X., Balsamo, G., Bechtold, P., Biavati, G., Bidlot, J.,
680 Bonavita, M., De Chiara, G., Dahlgren, P., Dee, D., Diamantakis, M., Dragani, R., Flemming, J., Forbes, R., Fuentes,
681 M., Geer, A., Haimberger, L., Healy, S., Hogan, R. J., Hólm, E., Janisková, M., Keeley, S., Laloyaux, P., Lopez, P.,
682 Lupu, C., Radnoti, G., de Rosnay, P., Rozum, I., Vamborg, F., Villaume, S., and Thépaut, J. N.: The ERA5 global
683 reanalysis, *Q. J. R. Meteorol. Soc.*, 146, 1999–2049, <https://doi.org/10.1002/qj.3803>, 2020.

684 Hua, W., Chen, Z. M., Jie, C. Y., Kondo, Y., Hofzumahaus, A., Takegawa, N., Chang, C. C., Lu, K. D., Miyazaki, Y., Kita,
685 K., Wang, H. L., Zhang, Y. H., and Hu, M.: Atmospheric hydrogen peroxide and organic hydroperoxides during
686 PRIDE-PRD'06, China: Their concentration, formation mechanism and contribution to secondary aerosols, *Atmos.*
687 *Chem. Phys.*, 8, 6755–6773, <https://doi.org/10.5194/acp-8-6755-2008>, 2008.

688 Jacob, D. J.: Heterogeneous chemistry and tropospheric ozone, *Atmos. Environ.*, 34, 2131–2159,
689 [https://doi.org/10.1016/S1352-2310\(99\)00462-8](https://doi.org/10.1016/S1352-2310(99)00462-8), 2000.

690 Jiang, Y. C., Zhao, T. L., Liu, J., Xu, X. D., Tan, C. H., Cheng, X. H., Bi, X. Y., Gan, J. B., You, J. F., and Zhao, S. Z.: Why
691 does surface ozone peak before a typhoon landing in southeast China?, *Atmos. Chem. Phys.*, 15, 13331–13338,
692 <https://doi.org/10.5194/acp-15-13331-2015>, 2015.

693 Kuhn-Régnier, A., Voulgarakis, A., Nowack, P., Forkel, M., Prentice, I. C., and Harrison, S. P.: The importance of
694 antecedent vegetation and drought conditions as global drivers of burnt area, 18, 3861–3879, [https://doi.org/10.5194/bg-](https://doi.org/10.5194/bg-18-3861-2021)
695 [18-3861-2021](https://doi.org/10.5194/bg-18-3861-2021), 2021.

696 Lefohn, A. S., Malley, C. S., Smith, L., Wells, B., Hazucha, M., Simon, H., Naik, V., Mills, G., Schultz, M. G., Paoletti, E.,
697 De Marco, A., Xu, X., Zhang, L., Wang, T., Neufeld, H. S., Musselman, R. C., Tarasick, D., Brauer, M., Feng, Z.,
698 Tang, H., Kobayashi, K., Sicard, P., Solberg, S., and Gerosa, G.: Tropospheric ozone assessment report: Global ozone
699 metrics for climate change, human health, and crop/ecosystem research, 6, <https://doi.org/10.1525/elementa.279>, 2018.

700 Lelieveld, J., Evans, J. S., Fnais, M., Giannadaki, D., and Pozzer, A.: The contribution of outdoor air pollution sources to
701 premature mortality on a global scale, *Nature*, 525, 367–371, <https://doi.org/10.1038/nature15371>, 2015.

702 Li, K., Chen, L., Ying, F., White, S. J., Jang, C., Wu, X., Gao, X., Hong, S., Shen, J., Azzi, M., and Cen, K.: Meteorological
703 and chemical impacts on ozone formation: A case study in Hangzhou, China, *Atmos. Res.*, 196, 40–52,
704 <https://doi.org/10.1016/j.atmosres.2017.06.003>, 2017.

705 Li, K., Jacob, D. J., Liao, H., Shen, L., Zhang, Q., and Bates, K. H.: Anthropogenic drivers of 2013–2017 trends in summer
706 surface ozone in China, *Proc. Natl. Acad. Sci. U. S. A.*, 116, 422–427, <https://doi.org/10.1073/pnas.1812168116>, 2019a.

707 Li, K., Jacob, D. J., Liao, H., Zhu, J., Shah, V., Shen, L., Bates, K. H., Zhang, Q., and Zhai, S.: A two-pollutant strategy for
708 improving ozone and particulate air quality in China, *Nat. Geosci.*, 12, 906–910, [https://doi.org/10.1038/s41561-019-](https://doi.org/10.1038/s41561-019-0464-x)
709 [0464-x](https://doi.org/10.1038/s41561-019-0464-x), 2019b.

710 Li, K., Jacob, D. J., Shen, L., Lu, X., De Smedt, I., and Liao, H.: Increases in surface ozone pollution in China from 2013 to
711 2019: Anthropogenic and meteorological influences, *Atmos. Chem. Phys.*, 20, 11423–11433,
712 <https://doi.org/10.5194/acp-20-11423-2020>, 2020.

713 Liu, Y. and Wang, T.: Worsening urban ozone pollution in China from 2013 to 2017 - Part 2: The effects of emission
714 changes and implications for multi-pollutant control, *Atmos. Chem. Phys.*, 20, 6323–6337, [https://doi.org/10.5194/acp-](https://doi.org/10.5194/acp-20-6323-2020)
715 [20-6323-2020](https://doi.org/10.5194/acp-20-6323-2020), 2020.

716 Lu, X., Zhang, L., and Shen, L.: Meteorology and Climate Influences on Tropospheric Ozone: a Review of Natural Sources,
717 Chemistry, and Transport Patterns, *Curr. Pollut. Reports*, 5, 238–260, <https://doi.org/10.1007/s40726-019-00118-3>,
718 2019a.

719 Lu, X., Zhang, L., Chen, Y., Zhou, M., Zheng, B., Li, K., Liu, Y., Lin, J., Fu, T. M., and Zhang, Q.: Exploring 2016–2017
720 surface ozone pollution over China: Source contributions and meteorological influences, *Atmos. Chem. Phys.*, 19,
721 8339–8361, <https://doi.org/10.5194/acp-19-8339-2019>, 2019b.

722 Ma, M., Gao, Y., Wang, Y., Zhang, S., Ruby Leung, L., Liu, C., Wang, S., Zhao, B., Chang, X., Su, H., Zhang, T., Sheng,
723 L., Yao, X., and Gao, H.: Substantial ozone enhancement over the North China Plain from increased biogenic emissions
724 due to heat waves and land cover in summer 2017, *Atmos. Chem. Phys.*, 19, 12195–12207, [https://doi.org/10.5194/acp-](https://doi.org/10.5194/acp-19-12195-2019)
725 19-12195-2019, 2019.

726 Mansfield, L. A., Nowack, P. J., Kasoar, M., Everitt, R. G., Collins, W. J., and Voulgarakis, A.: Predicting global patterns of
727 long-term climate change from short-term simulations using machine learning, *npj Clim. Atmos. Sci.*, 3,
728 <https://doi.org/10.1038/s41612-020-00148-5>, 2020.

729 McDonald, G. C.: Ridge regression, *Wiley Interdiscip. Rev. Comput. Stat.*, 1, 93–100, <https://doi.org/10.1002/wics.14>, 2009.

730 Meehl, G. A., Tebaldi, C., Tilmes, S., Lamarque, J. F., Bates, S., Pendergrass, A., and Lombardozzi, D.: Future heat waves
731 and surface ozone, *Environ. Res. Lett.*, 13, <https://doi.org/10.1088/1748-9326/aabdc6>, 2018.

732 Menze, B. H., Kelm, B. M., Masuch, R., Himmelreich, U., Bachert, P., Petrich, W., and Hamprecht, F. A.: A comparison of
733 random forest and its Gini importance with standard chemometric methods for the feature selection and classification of
734 spectral data, *BMC Bioinformatics*, 10, 1–16, <https://doi.org/10.1186/1471-2105-10-213>, 2009.

735 MEP: Ministry of Environmental Protection of the People’s Republic of China, Ambient Air Quality Standards (GB3095-
736 2012) (In Chinese), 2012.

737 Monks, P. S., Archibald, A. T., Colette, A., Cooper, O., Coyle, M., Derwent, R., Fowler, D., Granier, C., Law, K. S., Mills,
738 G. E., Stevenson, D. S., Tarasova, O., Thouret, V., Von Schneidmesser, E., Sommariva, R., Wild, O., and Williams,
739 M. L.: Tropospheric ozone and its precursors from the urban to the global scale from air quality to short-lived climate
740 forcer, *Atmos. Chem. Phys.*, 15, 8889–8973, <https://doi.org/10.5194/acp-15-8889-2015>, 2015.

741 Ning, G., Yim, S. H. L., Yang, Y., Gu, Y., and Dong, G.: Modulations of synoptic and climatic changes on ozone pollution
742 and its health risks in mountain-basin areas, *Atmos. Environ.*, 240, 117808,
743 <https://doi.org/10.1016/j.atmosenv.2020.117808>, 2020.

744 Nowack, P., Braesicke, P., Haigh, J., Abraham, N. L., Pyle, J., and Voulgarakis, A.: Using machine learning to build
745 temperature-based ozone parameterizations for climate sensitivity simulations, *Environ. Res. Lett.*, 13,
746 <https://doi.org/10.1088/1748-9326/aae2be>, 2018.

747 Nowack, P., Konstantinovskiy, L., Gardiner, H., and Cant, J.: Machine learning calibration of low-cost NO₂ and PM₁₀
748 sensors: Non-linear algorithms and their impact on site transferability, *Atmos. Meas. Tech.*, 14, 5637–5655,
749 <https://doi.org/10.5194/amt-14-5637-2021>, 2021.

750 Otero, N., Sillmann, J., Mar, K. A., Rust, H. W., Solberg, S., Andersson, C., Engardt, M., Bergström, R., Bessagnet, B.,
751 Colette, A., Couvidat, F., Cuvelier, C., Tsyro, S., Fagerli, H., Schaap, M., Manders, A., Mircea, M., Briganti, G.,
752 Cappelletti, A., Adani, M., D’Isidoro, M., Pay, M. T., Theobald, M., Vivanco, M. G., Wind, P., Ojha, N., Raffort, V.,
753 and Butler, T.: A multi-model comparison of meteorological drivers of surface ozone over Europe, *Atmos. Chem.*
754 *Phys.*, 18, 12269–12288, <https://doi.org/10.5194/acp-18-12269-2018>, 2018.

755 Ou, J., Yuan, Z., Zheng, J., Huang, Z., Shao, M., Li, Z., Huang, X., Guo, H., and Louie, P. K. K.: Ambient Ozone Control in
756 a Photochemically Active Region: Short-Term Despiking or Long-Term Attainment?, *Environ. Sci. Technol.*, 50,
757 5720–5728, <https://doi.org/10.1021/acs.est.6b00345>, 2016.

758 Pu, X., Wang, T. J., Huang, X., Melas, D., Zanis, P., Papanastasiou, D. K., and Poupkou, A.: Enhanced surface ozone during
759 the heat wave of 2013 in Yangtze River Delta region, China, *Sci. Total Environ.*, 603–604, 807–816,
760 <https://doi.org/10.1016/j.scitotenv.2017.03.056>, 2017.

761 Qi, J., Zheng, B., Li, M., Yu, F., Chen, C., Liu, F., Zhou, X., Yuan, J., Zhang, Q., and He, K.: A high-resolution air
762 pollutants emission inventory in 2013 for the Beijing-Tianjin-Hebei region, China, *Atmos. Environ.*, 170, 156–168,
763 <https://doi.org/10.1016/j.atmosenv.2017.09.039>, 2017.

764 Qu, K., Wang, X., Yan, Y., Shen, J., Xiao, T., Dong, H., Zeng, L., and Zhang, Y.: A comparative study to reveal the
765 influence of typhoons on the transport, production and accumulation of O₃ in the Pearl River Delta, China, *Atmos.*
766 *Chem. Phys.*, 21, 11593–11612, <https://doi.org/10.5194/acp-21-11593-2021>, 2021.

767 Shu, L., Wang, T., Han, H., Xie, M., Chen, P., Li, M., and Wu, H.: Summertime ozone pollution in the Yangtze River Delta
768 of eastern China during 2013–2017: Synoptic impacts and source apportionment, *Environ. Pollut.*, 257, 113631,
769 <https://doi.org/10.1016/j.envpol.2019.113631>, 2020.

770 Shu, L., Xie, M., Wang, T., Gao, D., Chen, P., Han, Y., Li, S., Zhuang, B., and Li, M.: Integrated studies of a regional ozone
771 pollution synthetically affected by subtropical high and typhoon system in the Yangtze River Delta region, China,
772 *Atmos. Chem. Phys.*, 16, 15801–15819, <https://doi.org/10.5194/acp-16-15801-2016>, 2016.

773 Sillman, S.: The relation between ozone, NO_x and hydrocarbons in urban and polluted rural environments, *Atmos. Environ.*,
774 [https://doi.org/10.1016/S1352-2310\(98\)00345-8](https://doi.org/10.1016/S1352-2310(98)00345-8), 1999.

775 Song, C., Liu, B., Dai, Q., Li, H., and Mao, H.: Temperature dependence and source apportionment of volatile organic
776 compounds (VOCs) at an urban site on the north China plain, *Atmos. Environ.*, 207, 167–181,
777 <https://doi.org/10.1016/j.atmosenv.2019.03.030>, 2019.

778 Squire, O. J., Archibald, A. T., Griffiths, P. T., Jenkin, M. E., Smith, D., and Pyle, J. A.: Influence of isoprene chemical
779 mechanism on modelled changes in tropospheric ozone due to climate and land use over the 21st century, *Atmos.*
780 *Chem. Phys.*, 15, 5123–5143, <https://doi.org/10.5194/acp-15-5123-2015>, 2015.

781 Stirnberg, R., Cermak, J., Kotthaus, S., Haeffelin, M., Andersen, H., Fuchs, J., Kim, M., Petit, J. E., and Favez, O.:
782 Meteorology-driven variability of air pollution (PM₁) revealed with explainable machine learning, *Atmos. Chem. Phys.*,
783 21, 3919–3948, <https://doi.org/10.5194/acp-21-3919-2021>, 2021.

784 [Tan, Z., Hofzumahaus, A., Lu, K., Brown, S. S., Holland, F., Huey, L. G., Kiendler-Scharr, A., Li, X., Liu, X., Ma, N., Min,](#)
785 [K. E., Rohrer, F., Shao, M., Wahner, A., Wang, Y., Wiedensohler, A., Wu, Y., Wu, Z., Zeng, L., Zhang, Y., and Fuchs,](#)
786 [H.: No Evidence for a Significant Impact of Heterogeneous Chemistry on Radical Concentrations in the North China](#)
787 [Plain in Summer 2014, *Environ. Sci. Technol.*, 54, 5973–5979, <https://doi.org/10.1021/acs.est.0c00525>, 2020.](#)

788 Wang, H., Wu, K., Liu, Y., Sheng, B., Lu, X., He, Y., Xie, J., Wang, H., and Fan, S.: Role of Heat Wave-Induced Biogenic
789 VOC Enhancements in Persistent Ozone Episodes Formation in Pearl River Delta, *J. Geophys. Res. Atmos.*, 126, 1–19,
790 <https://doi.org/10.1029/2020JD034317>, 2021.

791 Wang, N., Lyu, X., Deng, X., Huang, X., Jiang, F., and Ding, A.: Aggravating O₃ pollution due to NO_x emission control in
792 eastern China, *Sci. Total Environ.*, 677, 732–744, <https://doi.org/10.1016/j.scitotenv.2019.04.388>, 2019.

793 Wang, T., Xue, L., Brimblecombe, P., Lam, Y. F., Li, L., and Zhang, L.: Ozone pollution in China: A review of
794 concentrations, meteorological influences, chemical precursors, and effects, *Sci. Total Environ.*, 575, 1582–1596,
795 <https://doi.org/10.1016/j.scitotenv.2016.10.081>, 2017.

796 Wang, X. L.: Historical air quality data in China, available at: <https://quotsoft.net/air>, last access: 13 July 2021.

797 Wang, Y., Shen, L., Wu, S., Mickley, L., He, J., and Hao, J.: Sensitivity of surface ozone over China to 2000-2050 global
798 changes of climate and emissions, *Atmos. Environ.*, 75, 374–382, <https://doi.org/10.1016/j.atmosenv.2013.04.045>,
799 2013.

800 Wei, X., Lam, K. S., Cao, C., Li, H., and He, J.: Dynamics of the Typhoon Haitang Related High Ozone Episode over Hong
801 Kong, *Adv. Meteorol.*, 2016, <https://doi.org/10.1155/2016/6089154>, 2016.

802 Xie, X., Shao, M., Liu, Y., Lu, S., Chang, C. C., and Chen, Z. M.: Estimate of initial isoprene contribution to ozone
803 formation potential in Beijing, China, *Atmos. Environ.*, 42, 6000–6010,
804 <https://doi.org/10.1016/j.atmosenv.2008.03.035>, 2008.

805 Yang, L., Xie, D., Yuan, Z., Huang, Z., Wu, H., Han, J., Liu, L., and Jia, W.: Quantification of regional ozone pollution
806 characteristics and its temporal evolution: Insights from identification of the impacts of meteorological conditions and
807 emissions, *Atmosphere.*, 12, <https://doi.org/10.3390/atmos12020279>, 2021.

808 Young, P. J., Archibald, A. T., Bowman, K. W., Lamarque, J.-F., Naik, V., Stevenson, D. S., Tilmes, S., Voulgarakis, A.,
809 Wild, O., Bergmann, D., Cameron-Smith, P., Cionni, I., Collins, W. J., Dalsøren, S. B., Doherty, R. M., Eyring, V.,
810 Faluvegi, G., Horowitz, L. W., Josse, B., Lee, Y. H., MacKenzie, I. A., Nagashima, T., Plummer, D. A., Righi, M.,
811 Rumbold, S. T., Skeie, R. B., Shindell, D. T., Strode, S. A., Sudo, K., Szopa, S., and Zeng, G.: Pre-industrial to end 21st
812 century projections of tropospheric ozone from the Atmospheric Chemistry and Climate Model Intercomparison Project
813 (ACCMIP), *Atmos. Chem. Phys.*, 13, 2063–2090, <https://doi.org/10.5194/acp-13-2063-2013>, 2013.

814 Zhai, S., Jacob, D. J., Wang, X., Shen, L., Li, K., Zhang, Y., Gui, K., Zhao, T., and Liao, H.: Fine particulate matter (PM_{2.5})
815 trends in China, 2013-2018. separating contributions from anthropogenic emissions and meteorology, *Atmos. Chem.*
816 *Phys.*, 19, 11031–11041, <https://doi.org/10.5194/acp-19-11031-2019>, 2019.

817 Zhang, J., Gao, Y., Luo, K., Ruby Leung, L., Zhang, Y., Wang, K., and Fan, J.: Impacts of compound extreme weather
818 events on ozone in the present and future, *Atmos. Chem. Phys.*, 18, 9861–9877, [https://doi.org/10.5194/acp-18-9861-](https://doi.org/10.5194/acp-18-9861-2018)
819 2018, 2018.

820 Zhang, W., Zou, Y., Zheng, X. D., Wang, N., Yan, H., Chen, Y. P., Zhao, X. J., Ji, Z. P., Li, F., Mai, B. R., Yin, C. Q., Deng,
821 T., Fan, L. Y., and Deng, X. J.: Characteristics of the vertical distribution of tropospheric ozone in late autumn at

822 Yangjiang station in Pearl River Delta (PRD), China. PartI: Observed event, *Atmos. Environ.*, 244,
823 <https://doi.org/10.1016/j.atmosenv.2020.117898>, 2021.

824 Zhang, X., Fung, J. C. H., Lau, A. K. H., Hossain, M. S., Louie, P. K. K., and Huang, W.: Air quality and synergistic health
825 effects of ozone and nitrogen oxides in response to China’s integrated air quality control policies during 2015–2019,
826 *Chemosphere*, 268, 129385, <https://doi.org/10.1016/j.chemosphere.2020.129385>, 2021.

827 Zhao, X., Yu, B., Liu, Y., Chen, Z., Li, Q., Wang, C., and Wu, J.: Estimation of poverty using random forest regression with
828 multi-source data: A case study in Bangladesh, *Remote Sens.*, 11, 1–18, <https://doi.org/10.3390/rs11040375>, 2019.

829 Zheng, B., Tong, D., Li, M., Liu, F., Hong, C., Geng, G., Li, H., Li, X., Peng, L., Qi, J., Yan, L., Zhang, Y., Zhao, H., Zheng,
830 Y., He, K., and Zhang, Q.: Trends in China’s anthropogenic emissions since 2010 as the consequence of clean air
831 actions, *Atmos. Chem. Phys.*, 18, 14095–14111, <https://doi.org/10.5194/acp-18-14095-2018>, 2018.